

Contents lists available at ScienceDirect

Journal of Pharmaceutical Sciences

journal homepage: www.jpharmsci.org



Pharmacokinetics, Pharmacodynamics and Drug Transport and Metabolism

Probing the Mechanisms Underlying the Transport of the Vinca Alkaloids by P-glycoprotein



Gershon A.K. Mensah^a, Katherine G. Schaefer^b, Arthur G. Roberts^{a,*}, Gavin M. King^{b,c,*}, Michael G. Bartlett^{a,*}

- ^a Department of Pharmaceutical and Biomedical Science, University of Georgia, Athens, GA 30602, USA
- ^b Department of Physics and Astronomy, University of Missouri, Columbia, MO 65211, USA
- ^c Joint with Biochemistry, University of Missouri, Columbia, MO 65211, USA

ARTICLE INFO

Article history: Received 26 October 2023 Revised 18 March 2024 Accepted 18 March 2024 Available online 23 March 2024

Keywords: p-glycoprotein Vinca alkaloids Atomic force microscopy NMR Fluorescence spectroscopy

ABSTRACT

The efficacy of many cancer drugs is hindered by P-glycoprotein (Pgp), a cellular pump that removes drugs from cells. To improve chemotherapy, drugs capable of evading Pgp must be developed. Despite similarities in structure, vinca alkaloids (VAs) show disparate Pgp-mediated efflux ratios. ATPase activity and binding affinity studies show at least two binding sites for the VAs: high- and low-affinity sites that stimulate and inhibit the ATPase activity rate, respectively. The affinity for ATP from the ATPase kinetics curve for vinblastine (VBL) at the high-affinity site was 2- and 9-fold higher than vinorelbine (VRL) and vincristine (VCR), respectively. Conversely, VBL had the highest K_m (ATP) for the low-affinity site. The dissociation constants (K_Ds) determined by protein fluorescence quenching were in the order VBL < VRL< VCR. The order of the K_Ds was reversed at higher substrate concentrations. Acrylamide quenching of protein fluorescence indicate that the VAs, either at 10 μ M or 150 μ M, predominantly maintain Pgp in an open-outward conformation. When 3.2 mM AMPPNP was present, 10 μ M of either VBL, VRL, or VCR cause Pgp to shift to an open-outward conformation, while 150 μ M of the VAs shifted the conformation of Pgp to an intermediate orientation, between opened inward and open-outward. However, the conformational shift induced by saturating AMPPNP and VCR condition was less than either VBL or VRL in the presence of AMPPNP. At 150 μ M, atomic force microscopy (AFM) revealed that the VAs shift Pgp population to a predominantly open-inward conformation. Additionally, STDD NMR studies revealed comparable groups in VBL, VRL, and VCR are in contact with the protein during binding. Our results, when coupled with VAs-microtubule structure-activity relationship studies, could lay the foundation for developing next-generation VAs that are effective as anti-tumor agents. A model that illustrates the intricate process of Pgp-mediated transport of the VAs is presented.

© 2024 American Pharmacists Association. Published by Elsevier Inc. All rights reserved.

Introduction

Multidrug resistance (MDR) is a major obstacle hindering chemotherapy¹. The MDR phenotype has been observed in over 90% of cancer patients experiencing chemotherapeutic failures.² P-glycoprotein (Pgp), a well-studied member of the ATP binding cassette (ABC) superfamily, plays a pivotal role in the development of MDR.³ Pgp is a transmembrane transporter that expels a broad range of hydrophobic compounds, including drugs, from cells.⁴ Overexpression and activation of Pgp significantly contribute to MDR in tumor cells.⁵ Interestingly, both intrinsic overexpression of Pgp in tumor cells and induction of acquired MDR by certain anticancer agents have been observed.^{6,7} While numerous cellular signaling pathways facilitate

Pgp overexpression, reports also detail cell-to-cell transfer of Pgp in cancer and non-cancer cells.^{8,9} Multiple attempts have been made over the last three decades, with limited success, to address Pgp-mediated MDR.^{7,10} Although the use of specific Pgp inhibitors to enhance drug delivery showed early promise, their lack of specificity and high toxicity hindered success in clinical studies.^{7,11} Another approach involves designing anticancer drugs that can bypass the transporter.¹² However, this approach has not been fully realized due to a lack of comprehensive understanding regarding the structural and molecular mechanisms driving Pgp-mediated multidrug resistance. As a result, there has been considerable interest by pharmaceutical and regulatory agencies in understanding the structural and molecular factors that drive the Pgp-mediated transport of drugs.¹³

Vinca alkaloids (VAs), a class of drugs initially derived from the Catharanthus roseus plant endemic to Madagascar¹⁴, hold promise not only as anticancer agents but also for treating conditions like

mgbart@uga.edu (M.G. Bartlett).

^{*} Corresponding authors.

E-mail addresses: audie@uga.edu (A.G. Roberts), kinggm@missouri.edu (G.M. King),

diabetes and hypertension due to their hypoglycemic properties. 15 By binding to and disrupting mitotic spindle microtubule polymerization, VAs bring about cell cycle arrest at the M-phase and, corollary, cell deaths. 16,17 The influence of VAs extends to other cellular processes, including metabolism and biosynthesis of amino acids, lipids, and nucleic acids. 18 The VAs are one of the most-used class of anticancer agents due to their potential efficacy and include FDAapproved drugs such as vincristine (VCR), vinblastine (VBL), vinorelbine (VRL), vindesine (VDS), and vinflunine (VFL). 17,19 The VAs possess similar dimeric structures comprising an indole nucleus (catharanthine) and a dihydroindole nucleus (vindoline)²⁰ (Fig. 1). While binding studies between VAs and isolated microtubules suggest similar affinities^{21,22}, disparities arise when assessing their interference with tubulin formation in vitro, which indicates an order of VCR > VBL > VRL.^{22,23} In addition, the partition coefficient values of these drugs are not significantly different and could not account for the observed differences in their anticancer activities.²⁴ The puzzle deepens when considering cellular retention and potency. VCR displays a slower release rate and notably higher cellular retention than VBL.^{25,26} Similarly, VRL showcases a more significant volume distribution and enhanced cellular retention relative to VCR and VBL.²⁷ Interestingly, continuous treatment with either VBL or VCR yielded comparable cellular toxicity²⁸, implying a connection between cellular retention and anti-cancer potency. The discrepancy observed in the efficacy of the VAs is likely due to the activity of transmembrane transporters such as Pgp^{29,30} that reduces the cellular concentration

of the VAs. In fact, despite sharing a basic structure and being similarly lipophilic, in vitro studies using Caco-2 cells indicate Pgp-mediated efflux rate of 11.9, 8.5, and 4.7 for VBL, VCR, and VRL, respectively.31 The efflux rates of the VAs reduced significantly in the presence of Zosuquidar, a well-studied Pgp inhibitor, highlighting the crucial role Pgp plays in regulating the cellular retention of the VAs and, ultimately, their efficacy. Unfortunately, the underlying mechanisms driving the observed differences in Pgp-mediated transport rates of the VAs remain elusive. Any attempts aimed at developing the next generation of VAs without a comprehensive understanding of the underlying transport mechanism would remain a hit or miss. In this study, we provide structural and biochemical evidence for the Pgp-mediated transport of VAs. Drug-induced Pgp-mediated ATPase activities were investigated to identify plausible Pgp-ATP cooperativity since ATP hydrolysis drives the action of Pgp. The Pgp-drug affinity, another biochemical process that could dictate the activity of the protein, was investigated using drug-induced intrinsic tryptophan fluorescence quenching. STDD NMR was used to identify the functional groups in VAs likely involved in Pgp-drug interactions. Finally, drug-induced Pgp conformational changes were determined by acrylamide quenching of Pgp intrinsic tryptophan fluorescence spectroscopy and direct visualization via atomic force microscopy (AFM). Our results, coupled with previously published results, were used to build a simplified model that describes structural mechanisms underlying Pgp-mediated transport of VAs.

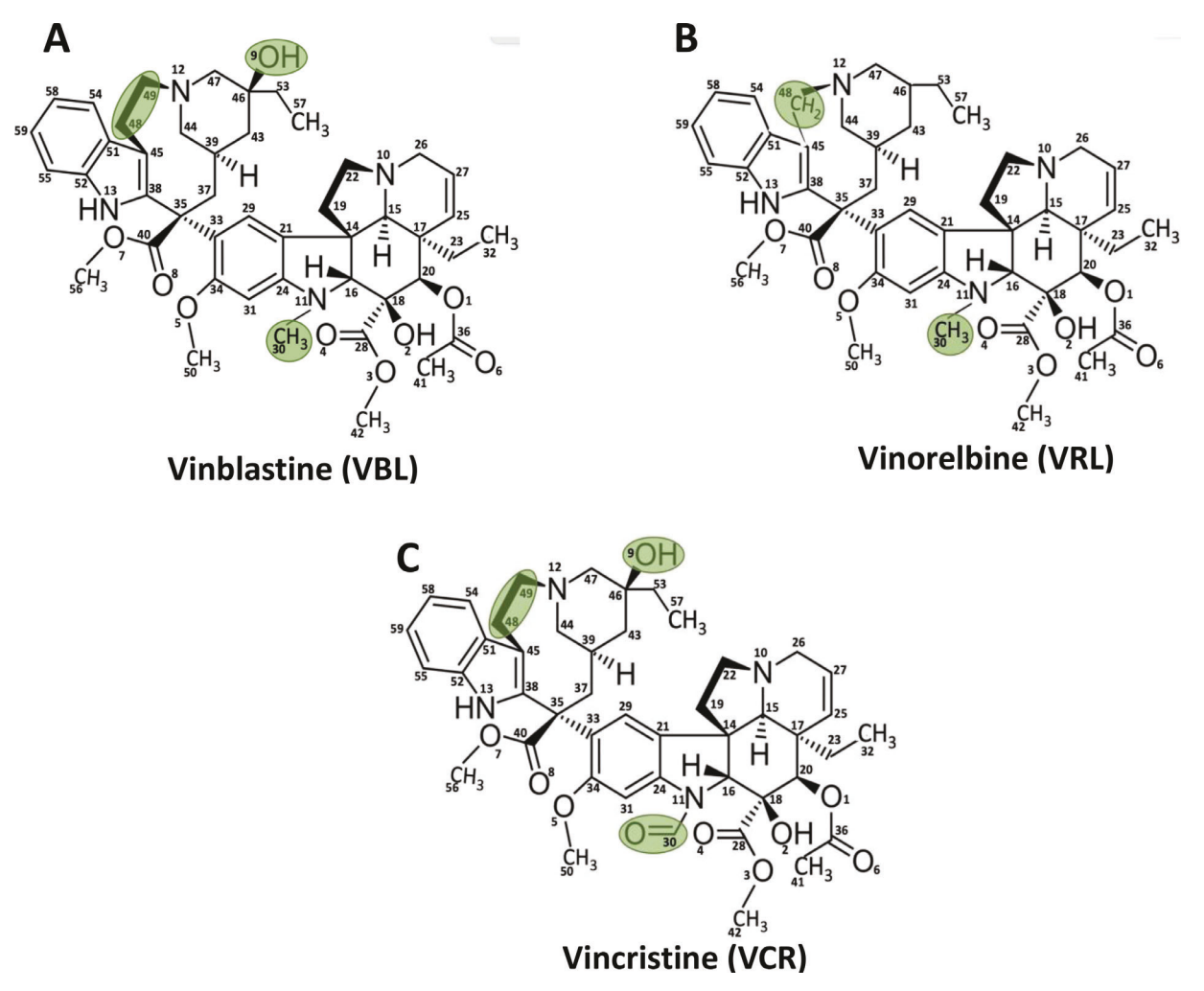


Fig. 1. The structure of Vinblastine (A), Vinorelbine (B), and Vincristine (C). The differences in the structure of the vinca alkaloids (VA) are highlighted in green.

Experimental Reagents and Methods

Chemicals and Reagents

VCR sulfate and VBL sulfate were procured from MP Biomedicals (Santa Ana, CA), while VRL was sourced from Astatech Inc. (Bristol, PA). Adenylyl-imido diphosphate lithium salt (AMPPNP), N-acetyl-Ltryptophanamide (NATA), and ammonium chloride (NH₄Cl) were obtained from Sigma Aldrich (Milwaukee, WI). The detergent utilized for protein purification, n-dodecyl- β -D-maltoside (DDM), was obtained from EMD Millipore Corporation (San Diego, CA). Sodium orthovanadate (Na₃OVO₃) was procured from Enzo Life Sciences (Farmingdale, NY). Magnesium chloride (MgCl₂) and sodium chloride (NaCl) were sourced from J.T Baker (Center Valley, PA). Disodium Adenosine triphosphate (Na₂ATP), cholesterol, and Tris hydrochloric acid were acquired from Amresco (Solon, OH). Dithiothreitol (DTT) was purchased from Gold Biotechnology (St. Louis, MO). Acrylamide and 4-(2-hydroxyethyl)-1-piperazineethanesulfonic acid (HEPES) were obtained from Calbiochem (San Diego, CA). Imidazole and ethylene glycol tetra-acetic acid (EGTA) were sourced from Alfa Aesar (Tewksbury, MA). Escherichia coli total lipid extract powder was procured from Avanti Polar Lipids Inc. (Alabaster, AL). Except otherwise stated, all other chemicals used in this study were purchased from Thermo Fisher Scientific (Waltham, MA).

Methods

Protein Expression and Purification

Pichia Pastoris engineered to overexpress his-tagged wild-type mouse Pgp (ABCB1A, MDR3) were cultured in glycerol-based media and further induced with methanol-based media to enhance the expression of proteins^{32,33} at the Bioexpression and Fermentation Facility (BFF), University of Georgia, Athens, GA. The cells were harvested and subjected to a repeated cycle of freezing, blending, and thawing. A two-step approach described previously³⁴ was adopted with some modifications to purify the protein. Initially, an affinity chromatography technique using nickel-nitrilotriacetic acid (Ni-NTA) (ThermoFisher Scientific, Waltham, MA) was conducted, followed by ion-exchange chromatography with Whatman DE52 diethylaminoethyl cellulose (DEAE) resin (ThermoFisher Scientific). The Purified Ppg solubilized in DDM were concentrated using Amicon Ultra-15 100 kDa cut-off filters (EMD Millipore, Billerica, MA). An SDS/PAGE analysis was done as previously described³² to assess the purity of the isolated protein. The purity was estimated to be greater than 95%. The concentration of the DDM-solubilized protein was determined with a Nanodrop (DeNovix, PHL), aliquots were made, and stored at -80°C.

Reconstitution of Pgp into liposomes

80% w/v Avanti E. coli total lipid extract and 20% w/v cholesterol were mixed in chloroform to a final concentration and volume of 10 mgmL⁻¹ and 10 mL, respectively. The organic mixture was dried using Buchi Rotavapor, Model R-114 (Buchi, DE). The dried film was then re-suspended in 10 mL of rehydration buffer (0.1 mM EGTA and 50 mM Tris-HCl, pH 7.4) to create a solution of liposomes with various sizes. Resuspension of the liposomes was facilitated by a freezethawed cycle using liquid nitrogen. Liposomes of varying sizes created by this approach were extruded at least 11x through a 400 nm cut-off filter installed on a LIPEX extruder instrument (Northern Lipids, Burnaby, British Columbia, Canada) to create homogeneously sized liposomes. Dynamic Light Scattering (DLS) was used to assess the sizes and uniformity of the extruded liposomes using Malvern Zetasizer Nano ZS (Malvern Instruments Ltd., UK). The DLS

chromatograms were analyzed with Zetasizer 7.03 software and showed homogenously sized liposomes with an average size of 250 nm

Pgp solubilized in detergent was dialyzed against HEPES buffer (20 mM HEPES, 100 mM NaCl, 5 mM MgCl₂, 2 mM DTT, pH 7.4) for 2 hours to remove residual detergents. The dialyzed Pgp was mixed with previously extruded liposomes to create a ratio of 0.16 mgmL⁻¹ liposomes per μ M of protein. The mixture was incubated on ice for 1 hour to promote protein integration into the liposomes before being dialyzed again on HEPES buffer for 2 hours to remove excess detergents and further enhance protein integration into the liposomes to form proteo-liposomes. The concentration of the proteo-liposomes was determined using a Bio-Rad DC Protein assay kit II, and aliquots were stored at -80°C in HEPES buffer (pH 7.4).

Pgp-mediated ATPase Activity

The Pgp catalytic cycle is an ATP-driven process that can be influenced by the presence of ligands.³⁵ As previously described, the Chifflet method was used to determine the rate of vanadate-sensitive Pgpmediated ATP hydrolysis.³⁶ In the Chifflet assay, the rate of ATP hydrolysis is indirectly detected by estimating the turnover of inorganic phosphate (Pi). Pi produced form complexes with molybdenum, which characteristically has a high absorbance at 850 nm. The ligandinduced ATPase activity assays for VBL, VCR, and VRL were carried out in Chifflet buffer (50 mM Tris-HCl, 150 mM NH₄Cl, 5 mM MgSO₄, 0.02% NaN₄, pH 7.4) with 250 nM of Pgp reconstituted into liposomes. Absorbance was detected on a Flexstation (III) spectrometer (Molecular Devices, Sunnyvale, CA) in a costar 96-well plate. If monophasic, the generated Pgp-mediated ATP hydrolysis kinetic curves were fit to a modified Michaelis-Menten equation that accounts for the basal activity (Eqn1).³⁷ The fitting was done with Python scripts developed in Igor Pro 6.2 software (Wavemetrics, Tigard, OR) to generate the kinetic parameters.

$$V = \frac{V_{max}[S]}{K_m + |S|} + Vbasal$$
 (1)

Where ν is the rate of ATP hydrolysis, V_{max} is the maximum rate of ATP hydrolysis, [S] is the substrate concentration, K_m is the Michaelis-Menten constant, and ν basal is the basal ATPase activity in the absence of drugs.

For biphasic ATP hydrolysis showing a second substrate inhibition site, the kinetic curves were fit into Eqn2 below to determine the kinetic parameters: inhibitory constant (K_i) , V_{max} , and K_m .

$$\nu = \frac{V_{max}}{1 + \frac{K_m}{|S|} + \frac{|S|}{K_i}} + \nu_{basal}$$
 (2)

Drug-Pgp Affinity Determined by Intrinsic Tryptophan Fluorescence Quenching

Tryptophan residues in a protein absorb and emit significantly around 280 nm and 330 nm, respectively. When ligands bind to a protein, they can alter the fluorescence intensity of the protein in an affinity-dependent manner by inducing changes in the local environment of the protein that house the tryptophan residues. Quenching of tryptophan residues in proteins has been exploited in earlier studies to determine the binding affinity of ligands such as drugs and nucleotides. In this study, the protein fluorescence emission was done using an Olis DM 45 spectrophotometer (Olis Corporation, Bogart, CA). A 10 nm band-pass filter was placed on the excitation and emission paths of the spectrophotometer to remove Rayleigh bands from the fluorescence emission spectra. The investigation was conducted on samples containing Chifflet buffer (pH 7.4), $1 \mu M$ of P-gp reconstituted into liposomes, and $2 \mu M$ DTT. The resultant ligand-induced fluorescence quenching data was corrected (Fcorrected) for

background, dilution, and inner filter effects with the Eqn3 below. 40,41

$$F_{corrected} = (F - B)10^{\frac{(\epsilon_{ex} b_{ex} + \epsilon_{em} b_{em})|Q|}{2}}$$
(3)

The measured protein fluorescence at 330 nm is represented as F, while B signifies the background, and [Q] denotes the ligand (quencher) concentration. The extinction coefficient of the ligand for excitation and emission wavelengths is represented as $\varepsilon_{\rm ex}$ and $\varepsilon_{\rm em}$, respectively. The extinction coefficients for the VAs were determined using previously described method. 42,43 The extinction coefficient ($\varepsilon_{\rm ex}$) values at 280 nm for VBL, VRL, and VCR were determined to be $4.19~\text{mM}^{-1}\text{cm}^{-1}$, $9.28~\text{mM}^{-1}\text{cm}^{-1}$, and 4.25~mmM⁻¹cm⁻¹, respectively. The path lengths along the excitation and emission axes are represented by bex and bem, respectively. The estimated emission extinction coefficients (ε_{em}) at 330 nm for VBL, VRL, and VCR were 0.631 mM⁻¹cm⁻¹, 2.79 mM⁻¹cm⁻¹, and 0.085 mM⁻¹cm⁻¹, respectively. Two main mechanisms typically underlie ligand-induced protein fluorescence quenching: static and dynamic quenching.⁴¹ In static quenching, ligands form complexes with the protein, while dynamic fluorescence quenching arises from random collisions between the protein and ligand. The effect of two or more different temperatures (25°C, 30°C, 37° C) on the fluorescence quenching curve was used to identify the predominant quenching mechanism present. When dynamic quenching is predominant, elevated temperatures increase collision frequency, resulting in higher K_{sv} values. In contrast, for static quenching, higher temperatures decrease the residency time of the ligand-protein complex, yielding lower Ksv values. The VAs showed a biphasic curve, exhibiting static quenching and dynamic mechanisms at relatively low and high concentrations, respectively. However, in the presence of saturating AMPPNP, the VAs showed a monophasic quenching curve, which was determined to be primarily static (results not shown). In the case of monophasic fluorescence quenching, the corrected fluorescence (Fcorrected) quenching curves were fitted to a Stern-Volmer equation below (Eqn4) to determine the Stern-Volmer constant

$$F_{corrected} = \frac{F_{o(corrected)}}{1 + K_{sv}[Q]} + F_{unquenched}$$
(4)

Here, the F_o (corrected) represents the fluorescence in the absence of a quenching ligand, F unquenched is an offset related to unquenched fluorescence, and [Q] is the concentration of the ligand. Conversely, fluorescence quenching curves showing biphasic characteristics were fitted to a modified Stern-Volmer equation (Eqn 5)

$$F_{corrected} = \frac{F_{o,H}}{1 + K_{sv,H}[Q]} + \frac{F_{o,L}}{1 + K_{sv,L}[Q]} + F_{unquenched}$$
 (5)

The amplitudes of protein fluorescence at low and high ligand concentrations are denoted as $F_{o,L}$, and $F_{o,H}$, respectively. Correspondingly, the K_{sv} values for the low and high ligand concentrations are represented as $K_{sv,H}$ and $K_{sv,L}$, respectively.

Drug-induced Pgp Conformational Changes Probed by Acrylamide Quenching

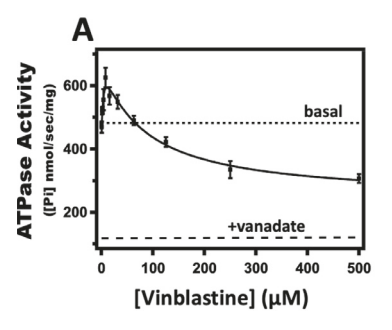
Acrylamide is a small polar quencher that can effectively quench the fluorescence emitted by tryptophan residues within proteins via collision. ⁴¹ Data from prior studies suggests that proteins can undergo changes in their conformation when they interact with ligands. ⁴⁴ These conformational changes could either occlude or expose the tryptophan residues in the protein, leading to changes in the proportion of solvent-accessible tryptophan

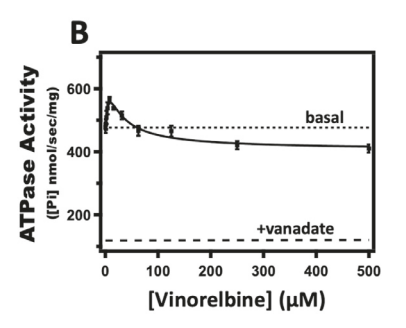
residues. 40,45 As acrylamide is unable to penetrate the hydrophobic core of the protein easily, alterations in the protein's fluorescence can provide insights into potential modifications in the protein's tertiary structure induced by ligands. 46 In this study, as acrylamide was titrated against the sample solution, the fluorescence intensity was measured at 330 nm, following excitations at 280 nm. The sample solution consists of 1 μ M Pgp reconstituted into liposomes in Chifflet buffer supplemented with 2 mM DTT. The fluorescence intensities were corrected with Eqn3, and a Stern-Volmer plot of $F_{o(corrected)}/F_{(corrected)}$ against the acrylamide concentration was generated. The slope of the Stern-Volmer curve is a function of the degree of quenching, and it is related to the K_{sv} value by Eqn6 below 41 :

$$\frac{F_{o(corrected)}}{F_{(corrected)}} = 1 + K_{sv}[Q] \tag{6}$$

Saturation Transfer Double Difference (STDD) NMR

STDD NMR is a powerful ligand-focused technique used to study ligand-receptor interactions and epitopes mapping. 47,48 Thus, STDD NMR can be used to identify the functional groups on ligands that are in either direct or near-direct contact with the protein. The principle of STD NMR involves selectively applying a long, low-power pulse that saturate the protons of the receptor.⁴ When a ligand binds to the receptor, protons of the ligands within \sim 5 Å from the saturated protein experience significant saturation transfer from the receptor.⁴⁹ Upon dissociation, the saturation transferred to the ligand is detected as saturation transfer difference (STD). The degree of saturation transferred inversely corresponds to the ligand-receptor distance and reflects the strength of the interaction. Since many Pgp substrates are highly lipophilic, nonspecific interactions between ligands and liposomes can interfere with observed STD NMR spectra. The STD NMR spectrum of the drug in the presence of liposomes was subtracted from the STD ¹H NMR spectrum of the ligand with proteins reconstituted into liposomes to account for potential STD contributions from ligand-liposome interactions. This subtraction leads to a saturation transfer double difference (STDD) spectrum. 50,51 This approach was employed to investigate the functional groups of VBL, VCR, and VRL potentially involved in Pgp-drug interactions. All NMR experiments were conducted at 25°C (unless stated otherwise) on a Varian INOVA 600 MHz NMR spectrometer equipped with a ¹Hdetect broadband probe {HX}. Data analyses were performed with iNMR software (Nucleomatic, Molfetta, Italy), Igor Pro 6.2, and Mnova 14.2.0 (Mastrelab Research S.L, Santiago de Compostela, Spain). The STDD NMR procedure in this study was performed as previously described⁵² with some modifications. 100 mM potassium phosphate buffer (80% D₂O, 20% ddH2O, pH 7.4) containing 1 μ M Pgp reconstituted into liposomes, and 1 mM of either VBL, VRL or VCR were prepared. Control samples were similarly prepared with liposomes instead of Pgp-reconstituted liposomes. A Water Suppression by Gradient Tailored Excitation (WATERGATE) gradient pulse sequence was used to suppress water signals that would have otherwise dwarfed the signals from the ligand.⁵³ Selective excitation and saturation of the protein were achieved using a 50 ms train of Gaussian-shaped selective pulses for 2s, followed by a delay of 5s to enable relaxation.^{47,54} STD NMR spectra were obtained through phase cycling by alternating Pgp irradiation resonance between -1.5 ppm (on resonance) and 42 ppm (off-resonance) for 512 scans. Subtracting the off-resonance from the on-resonance spectra generated the STD 1H NMR spectrum. Control experiments were conducted under the same conditions and subtracted from the ¹H STD NMR spectrum of the





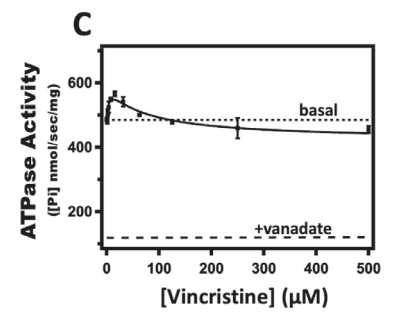


Fig. 2. The effect of the vinca alkaloids on Pgp-mediated ATP hydrolysis. Ligand-induced Pgp-coupled ATPase activity in the presence of increasing concentrations of (A) VBL (closed squares), (B) VRL (closed squares), and (C) VCR (closed squares). For comparison, the basal and vanadate-inhibited ATPase activity are shown as dotted lines and dashed lines, respectively, in each panel. Each data point represents the average of at least 3 independent experiments, and the error bars shown represent the standard deviation.

reconstituted Pgp sample with the drug, yielding the STDD 1H NMR spectrum. The observed difference (Δl) directly reflects the strength of the interaction between drug functional groups and the protein. The STDD amplification factor was calculated using Eqn7^{34,54} below.:

STDD Amplication Factor =
$$\frac{[I]}{[P]} \frac{\Delta I}{I_0}$$
 (7)

Where *Io* represents the amplitude of the 1H NMR peaks, [I] denotes the ligand concentration, and [P] is the protein concentration.

Atomic Force Microscopy

Atomic force microscopy (AFM) is a robust technique initially developed to examine the physical characteristics of solid-state materials by directly probing their surfaces with a mechanical probe.⁵⁵ This technique has been adopted in earlier studies to analyze protein dynamics and structure, facilitating the identification of ligand-induced conformational changes in proteins. 38,56 The changes in the conformation of a protein prior and after the addition of ligands, as determined by AFM, can provide insights into the effect of ligand-binding on the structure of the protein. In the present study, a solution of Pgp reconstituted into liposomes (proteoliposomes) was diluted in imaging buffer (20 mM HEPES, 100 mM NaCl, 5 mM MgCl₂; pH 7.4) to 100 nM. About 90 μL of this solution was deposited onto a clean coverslip (Corning, Corning, NY) and incubated at 25°C for approximately 30 minutes. The incubation led to the rupture of proteoliposomes, forming a planar lipid bilayer atop the glass surface. The samples were rinsed with 90 μ L of buffer at least 5 times using a buffer exchange technique. AFM imaging of the EC-side and C-side domains of Pgp protrusions above the lipid bilayer was performed as previously described.⁵⁷ For each of the selected VAs under study, AFM imaging of the ligand-free Pgp (apoPgp) was performed first, followed by the addition of 150 μM of either VBL, VRL, or VCR. AFM imaging was repeated upon the addition of ligands such that a nominally similar area of the sample was captured. Only particles that could be positively assigned as either EC or C-side domain features of Pgp were analyzed. AFM images were obtained in imaging buffer at ~30°C in tapping mode with Biolever mini tips (BL-AC40TS, Olympus, Tokyo, Japan) installed on a commercial instrument (Asylum Research Cypher, Santa Barbara, CA). A tip-sample force < 100 pN were used to minimize the probability of protein distortion. AFM images were analyzed using custom software developed in Igor Pro 7 (Wavemetrics, Portland, OR) as previously reported.⁵⁷ The smoothed histograms were constructed in Igor Pro 7 using kernel density estimation with Epanechnikov kernels.⁵⁸

Results

Modulation of Pgp-mediated ATPase activity

The Pgp catalytic cycle is an energy-dependent process^{59,60} that requires at least one ATP molecule per VA molecule transported. 61 Thus, the rate of ATP hydrolysis can be a good indicator of the activity of the protein. Fig. 2 shows the effect of selected VAs on Pgp-mediated ATP hydrolyses. Panels 2A, 2B, and 2C show the kinetic curves of drug-induced Pgp-mediated ATPase activity in the presence of increasing concentrations of VBL, VRL, and VCR, respectively. The observed basal activities of Pgp in the absence of VBL, VRL, and VCR (dashed lines) were similar, averaging 477 \pm 22 nmolmin⁻¹mg⁻¹, which is consistent with previous estimates.⁶² Drug-induced Pgpmediated ATP-hydrolyses kinetic curves deduced for all the tested compounds were biphasic, implying that at least two distinct ratelimiting steps or mechanisms are involved. The two phases consist of substrate stimulation at lower drug concentrations ($< 20 \mu M$), reaching maximum activation of 35%, 18%, and 16% over the basal activity level for VBL, VRL, and VCR, respectively. ATPase activation was followed by inhibition at higher concentrations, reducing the maximum activity induced by VBL, VRL, and VCR by 51%, 27%, and 24%, respectively. Previous studies have observed similar Pgp binding modes for the VAs. 63-66 The kinetic curves generated were fit to a modified Michaelis-Menten equation for biphasic interactions, with second substrate inhibition (Eqn2) to determine the kinetic parameters such as V_{max} , K_m , and K_i values. The K_m and K_i deduced for VBL (Fig. 2A) were 1.78 \pm 2.34 μ M and 24.17 \pm 6.12 μ M, respectively. These values are in agreement with a previous report where a biphasic kinetic curve was observed.⁶⁷ On the contrary, in another study where only the inhibitory phase of the curve was observed (probably due to the concentration of the drug used) the K_m(ATP) induced by VBL was substantially different. 68 The apparent V_{max} extracted from the VBLinduced ATPase kinetics curve was 601 \pm 30 nmolmin⁻¹mg⁻¹. The K_{m} , K_{i} , and V_{max} values generated from the VRL-induced ATPase kinetic fit (Fig. 2B) were 5.12 \pm 3.87 μ M, 8.79 \pm 4.76 μ M, and 590 \pm 21 nmolmin⁻¹mg⁻¹, respectively. For VCR (Fig. 2C), the estimated K_m and K_i values were 17.04 \pm 6.50 μ M and 7.40 \pm 3.26 μ M. The associated V_{max} for the VCR was 558 \pm 33 nmolmin⁻¹mg⁻¹. Overall, these results aligns well with previous studies that suggest that VAs act as both Pgp substrate and inhibitor of Pgp-coupled ATP hydrolysis depending on the availing concentrations.^{67,69} However, unlike verapamil, which almost completely inhibits Pgp activity at 50 μ M⁷⁰ with an average K_i of 1.9 \pm 0.5 μ M³⁴, the degree of inhibition by VAs is relatively mild and may fall outside of physiological relevant dose.⁷¹ In addition, the VAs have relatively high non-target toxicity, making their usage as a potential inhibitor untenable. A summary of the kinetic data generated from VA-induced Pgp-mediated ATPase is shown in Table S1.

Pgp-Ligand Binding Affinity Probed by Protein Fluorescence Quenching

Fluorescence changes in proteins caused by drug interactions with tryptophan residues in or near the drug-binding pocket can be a valuable tool for assessing drug-protein binding affinity.³⁹ Following previous works^{40,72}, Fig. 3 shows the effect of the VAs on Pgp fluorescence. Panels 3A, 3C, and 3E represent the spectra of VA-induced Pgp emission decay observed between 300 nm and 500 nm.

Pgp fluorescence emission spectra showed a maximum at 330 nm following excitation at 280 nm. The upper and lower thick black lines show the maximum and minimum protein fluorescence observed in the absence and presence of 150 μ M of drugs, respectively. The grey lines represent the spectra between the maximum and minimum protein fluorescence. The maximum protein fluorescence observed at 330 nm decreased by approximately 55%, 40%, and 32% in the presence of 150 μ M of VBL, VRL, and VCR, respectively. In the presence of

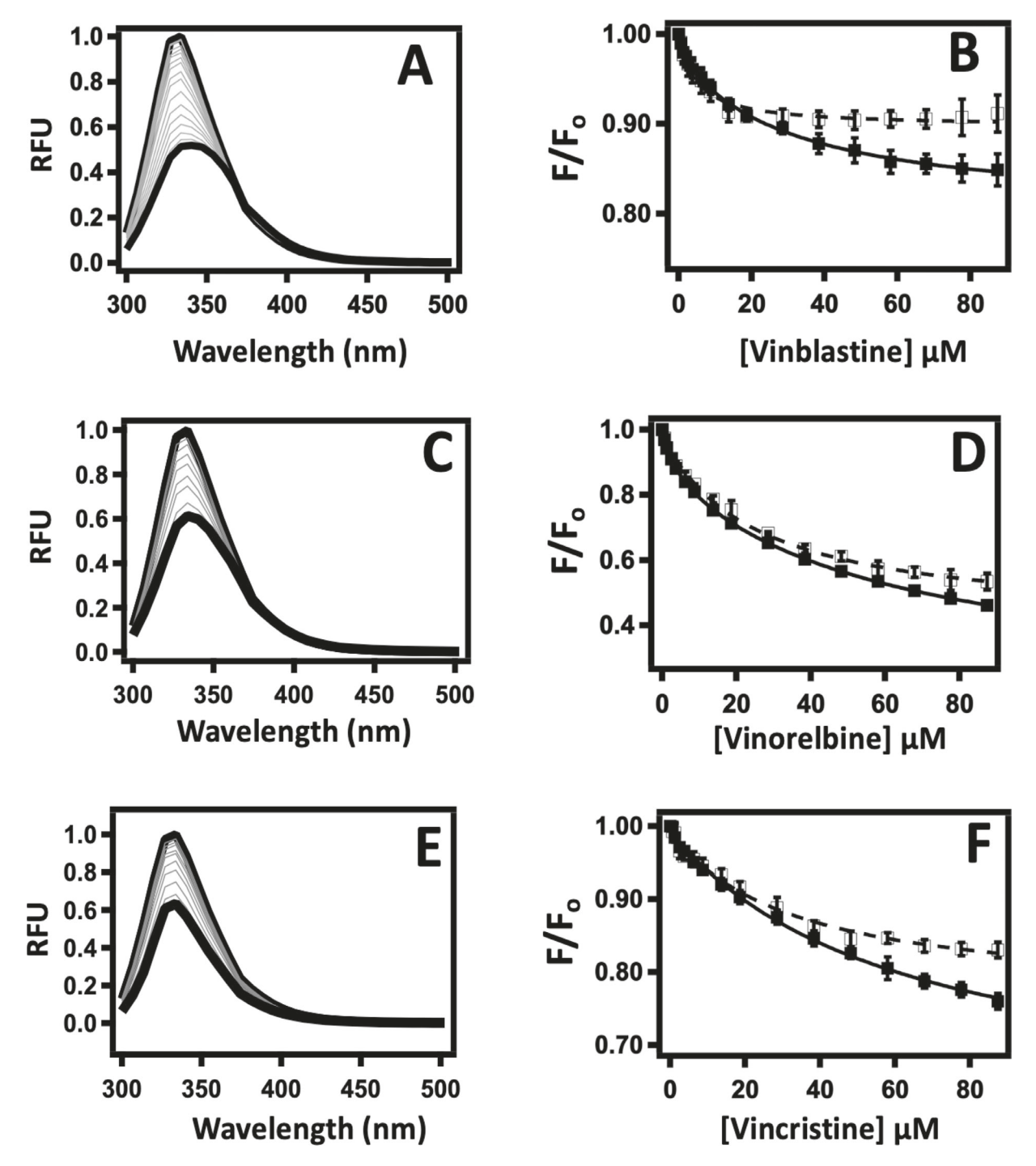


Fig. 3. The binding affinity of vinca alkaloids to Pgp determined by the ligand-induced quenching of intrinsic tryptophan fluorescence. A normalized Fluorescence emission decay spectra of Pgp following excitation at 280 nm in the presence of increasing (A) VBL, (C) VRL, and (E) VCR concentrations. The upper and lower thick lines represent the absence (0 μ M) and the presence of saturating concentrations (150 μ M) of the VAs. The fluorescence spectra at the intermediate concentrations are shown in gray lines between the thick lines. The corrected fluorescence emission amplitudes at 330 nm were plotted as a function of the concentration of (B) VBL, (D) VRL, and (F) VCR in the absence (closed square) and presence (opened square) of saturating (3.2 mM) AMPPNP. Each data point and error bar represent the average and standard deviation of at least three independent experiments.

saturating AMPPNP, 150 μ M of VBL induced about 34% decrease in protein fluorescence (not shown). Similarly, VCR and VRL decreased the protein's fluorescence by 30% and 38%, respectively, in the presence of saturating AMPPNP (not shown). The amplitudes of Pgp fluorescence were monitored at 330 nm as either VBL, VRL, or VCR was titrated against the protein and the resulting fluorescence amplitudes were adjusted for the inner filter effect using Eqn3. The corrected fluorescence amplitudes, F(corrected), generated were plotted against the corresponding concentration of VBL (Fig. 3B), VCR (Fig. 3D), and VRL (Fig. 3F) in the absence (closed squares) and presence (opened squares, dashed lines) of saturating AMPPNP. Pgp fluorescence quenching curves for the VAs were biphasic: a high-affinity phase at relatively low drug concentrations and low affinity at high concentrations. The K_{sv} values were determined by fitting the curves to Eqn5 for a biphasic binding curve. In the presence of saturating AMPPNP, the generated Pgp fluorescence quenching curves for the VAs were monophasic and were fit to Eqn4 to determine the apparent K_{sv} values. The K_{D,H} and K_{D,L} values for Pgp-drug interactions were determined from their respective $K_{sv,H}$ and $K_{sv,L}$ values obtained from the protein fluorescence curves. The K_{sv} and K_D values for Pgp-VAs interactions are summarized in Table S2. The K_{sv,H} and K_{D,H} values for VBL were 0.849 \pm 0.06 μM^{-1} and 1.18 \pm 0.07 $\mu \text{M},$ respectively, which are within the range previously reported. 64,73 The K_{sv,L} and $K_{D,L}$ for VBL were 0.015 \pm 0.004 μM^{-1} and 67.67 \pm 5.08 μM , respectively. In the presence of saturating AMPPNP, a monophasic fluorescence binding curve was observed for VBL, resulting in K_{sv} and K_D values of 0.052 \pm 0.006 μM^{-1} and 19.26 \pm 2.25 μM , respectively. Similarly, the K_{sv,H} and K_{sv,L} values deduced for Pgp-VRL interactions were 0.393 \pm 0.087 μM^{-1} and 0.032 \pm 0.01 μM^{-1} , respectively. The corresponding $K_{D,H}$ and $K_{D,L}$ values for VRL were 2.55 \pm 0.16 μ M and 30.96 \pm 5.16 μ M for the high- and low-affinity binding sites on Pgp. The K_{sv} and K_D values deduced from the interaction between VRL and Pgp in the presence of saturating AMPPNP were 0.040 \pm 0.019 μ M⁻¹ and 25.00 \pm 2.49 μ M, respectively. The Pgp-VCR interactions also exhibited two distinct binding affinities, with K_{D,H}, and K_{D,L} values of $3.84 \pm 0.61~\mu\text{M}$ and $24.89 \pm 5.64~\mu\text{M}$, respectively. These K_D values were derived from the VCR-induced K_{sv,H} and K_{sv,L} values, estimated to be 0.26 \pm 0.028 μM^{-1} and 0.040 \pm 0.003 μM^{-1} , respectively. These results agree with previously reported data suggesting a high and low-affinity uptake of VCR by Pgp-containing membrane vesicles.⁶⁶ AMPPNP shifted VCR into a monophasic binding curve with K_{sv} and K_{D} values of 0.104 \pm 0.038 μM^{-1} and 9.58 \pm 3.51 μM , respectively.

Ligand-induced Conformational Changes in Pgp Probed by the Acrylamide Quenching of Protein Fluorescence

Pgp is a conformationally dynamic protein whose catalytic cycle samples between open-inward to open-outward conformations. Pgp-mediated transport of ligands is believed to be modulated by these conformational changes in the protein. 41,74 Changes in the overall structure of a protein may also affect the accessibility of tryptophan residues within the protein. Ligand-induced conformational changes in proteins have been estimated previously by probing the changes in relative exposure of solvent-accessible tryptophan residues within the protein before and after the addition of ligands. 75–77 In this study, acrylamide quenching of readily accessible tryptophan residues was used to investigate the underlying ligand-induced conformational changes in the Pgp that modulate the transport of the VAs by the transporter. The degree of acrylamide quenching is typically most pronounced when Pgp is in an open-inward conformation, where the tryptophan residues within or near the binding pockets are easily accessible by the surrounding solvent. Conversely, acrylamide quenching is minimal in the open-outward conformation due to the shielding of the solvent-accessible tryptophan residues. Fig. 4 shows the Stern-Volmer plots illustrating the quenching of Pgp fluorescence by acrylamide in the presence of the selected VAs under study. The slopes obtained from these curves, which are equivalent to the K_{sv} values, provide an estimate of the extent of quenching. Changes in the estimated K_{sv} value indicate a shift in the protein's tertiary structure, influencing the number of solvent-accessible tryptophan residues. Fig. 4A presents the Stern-Volmer plot of NATA (Fig. 4A, opened circle) and Pgp (Fig.4A, opened squares) in the absence of ligands (apoPgp). The K_{sv} values were determined by fitting the curve into Eqn6 after accounting for the inner filter effect, dilution, and background with Eqn3 and are summarized in Table S3. The estimated K_{sv} values for NATA (a free tryptophan analog) and apoPgp were 31.54 \pm 2.19 M⁻¹ and 4.17 \pm 0.15 M⁻¹, respectively. Had all the tryptophan residues in the protein been solvent-accessible, the estimated K_{sv} value of apoPgp would have been expected to match that of NATA. However, since acrylamide quenching of the tryptophan residues are only feasible when the distance between the fluorophore and the quencher is $< 3 \text{ Å}^{78}$, most of the tryptophan residues in Pgp are likely buried within the hydrophobic region of the protein and are not readily solvent accessible.⁷⁹ In fact, reports suggests that only 3 out of the 11 tryptophan residues in Pgp are likely completely solvent-accessible.⁷⁹ Note that the solved x-ray structure of mammalian apoPgp and other analogous bacterial transporters showed the protein in an open-inward conformation.^{80,81} Subsequently, it was assumed that the K_{sv} value of apoPgp represents the protein in an open-inward conformation, where the two nucleotidebinding domains (NBDs) are apart. In the presence of saturating AMPPNP, the K_{sv} value of Pgp decreased to 1.99 \pm 0.04 M^{-1} (Fig. 4B. closed triangle), suggesting a shift to the open-outward conformation where the fluorescence residues are relatively occluded from the bulk solvent. This inference is based on reports showing an open-outward conformation in X-ray crystal and cryo-EM structures of Pgp in the presence of nucleotides.^{82,83} Stern-Volmer's plots of Pgp in the presence of 10 μ M of VBL, VRL, and VCR are presented in panels 4C, 4E, and 4G. These plots (as well as 4D, 4F, and 4H) compare the fluorescence quenching in the absence (closed square) and presence (opened square) of 3.2 mM AMPPNP. The estimated K_{sv} values deduced from the Stern-Volmer plots of Pgp in the presence 10 μ M of either VBL, VRL, or VCR were 3.87 \pm 0.16 M⁻¹, 3.91 \pm 0.35 M⁻¹, and $4.02 \pm 0.15 \text{ M}^{-1}$, respectively, which suggest that the binding of VAs to Pgp at low concentrations does not significantly influence the conformation of the protein. In the presence of saturating AMPPNP, however, the K_{sv} value obtained for the VAs at 10 μ M decreased considerably to 1.84 \pm 0.03 M⁻¹, 2.04 \pm 0.05 M⁻¹, 2.58 \pm 0.07 M⁻¹ for VBL, VRL, and VCR, respectively. In the presence of 150 μ M of VBL, VRL, and VCR, the K_{sv} values deduced from the Stern-Volmer's plot of Pgp fluorescence were 3.94 \pm 0.19 M⁻¹, 4.10 \pm 0.05 M⁻¹, and 4.30 \pm 0.12 M $^{-1}$, respectively. The K_{sv} values induced by 150 μ M VBL, VRL, and VCR decreased significantly to 2.75 \pm 0.047 M⁻¹, 2.85 \pm 0.08 M^{-1} , 3.6 \pm 0.09 M^{-1} , respectively, in the presence of saturating AMPPNP. Taken together, these results suggest that the binding of nucleotides induces the conformational shift in Pgp necessary for transport.

Identification of Ligand-Receptor Interactions by STDD NMR

STD NMR is a robust spectroscopic technique that can be used to study the interactions between proteins and ligands in solution. ^{49,84} In this study, we employed the STDD NMR technique to investigate the specific moieties on VAs that likely interact with Pgp. Fig. 5 displays the STDD NMR spectra, highlighting the protein-ligand interactions between the VAs and Pgp. Panels 5A, 5C, and 5E show the 1D ¹H STDD NMR spectra for VBL, VRL, and VCR, respectively. STDD spectra for the VAs were compared with their respective 1D ¹H spectra (data not shown) to identify and assign the peaks that showed significant

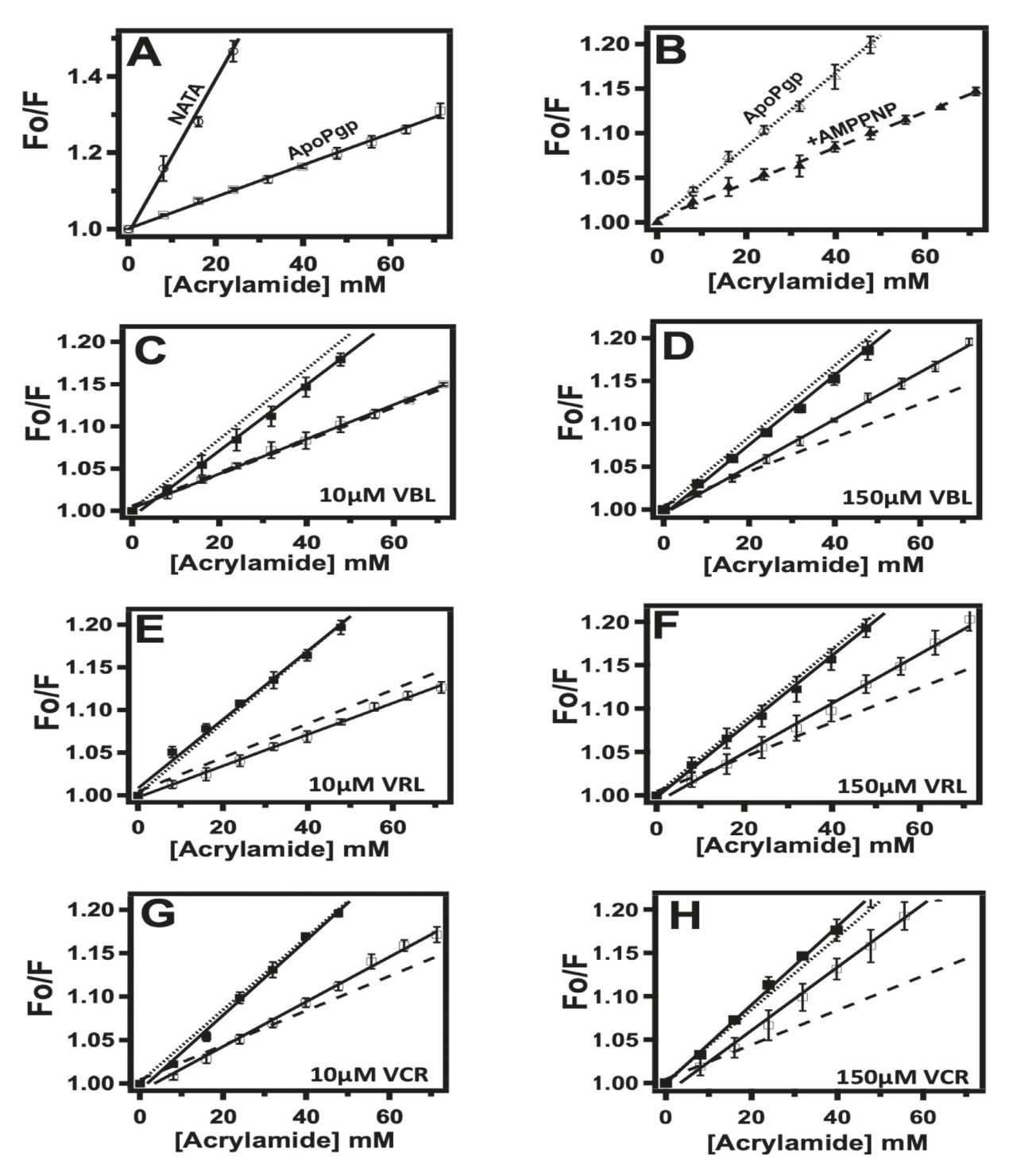


Fig. 4. Vinca alkaloid-induced conformational changes in Pgp probed by acrylamide quenching of protein fluorescence. (A) Stern-Volmer plot for NATA (open circles) and apoPgp (open squares). (B) Stern-Volmer plot for Pgp fluorescence in the absence (open triangle, dotted line) and presence of 3.2 mM AMPPNP (closed triangle, dashed line). Panels (C) and (D) depict the fitted Stern-Volmer plots of Pgp induced by $10~\mu\text{M}$ and $150~\mu\text{M}$ of VBL, both in the absence (closed square) and presence (open square) of 3.2~mM AMPPNP. (E) $10~\mu\text{M}$ and (F) $150~\mu\text{M}$ VRL-induced Stern-Volmer plots of Pgp fluorescence in the absence (closed square) and presence (open square) of 3.2~mM AMPPNP. For comparison, Stern-Volmer plots of apoPgp without (dotted lines) and with AMPPNP (dashed lines) are shown in panels C-H. Data points and error bars represent the mean and standard deviation, respectively, from a minimum of three independent experiments.

STDD. The 1D ¹H spectra observed for the VAs under study were consistent with previously reported studies. ^{85–87} Due to their relatively large molecular sizes, the VAs exhibited substantial STDD NMR signals from various functional groups. Interestingly, identical groups on VBL, VRL, and VCR displayed significant STDD NMR signal amplitudes, with the highest peaks originating from the methyl groups.

Specifically, signals from C_{42} , C_{41} , and C_{56} (see Fig. 1) displayed the highest amplitudes for VBL, VRL, and VCR, respectively. The data obtained from the STDD NMR spectrum were fit to Eqn7 to calculate the amplification factor, which normalizes the STDD amplitudes and accounts for multiple protons giving rise to a single peak. Category plots of STDD amplification factors estimated for VBL, VRL, and VCR

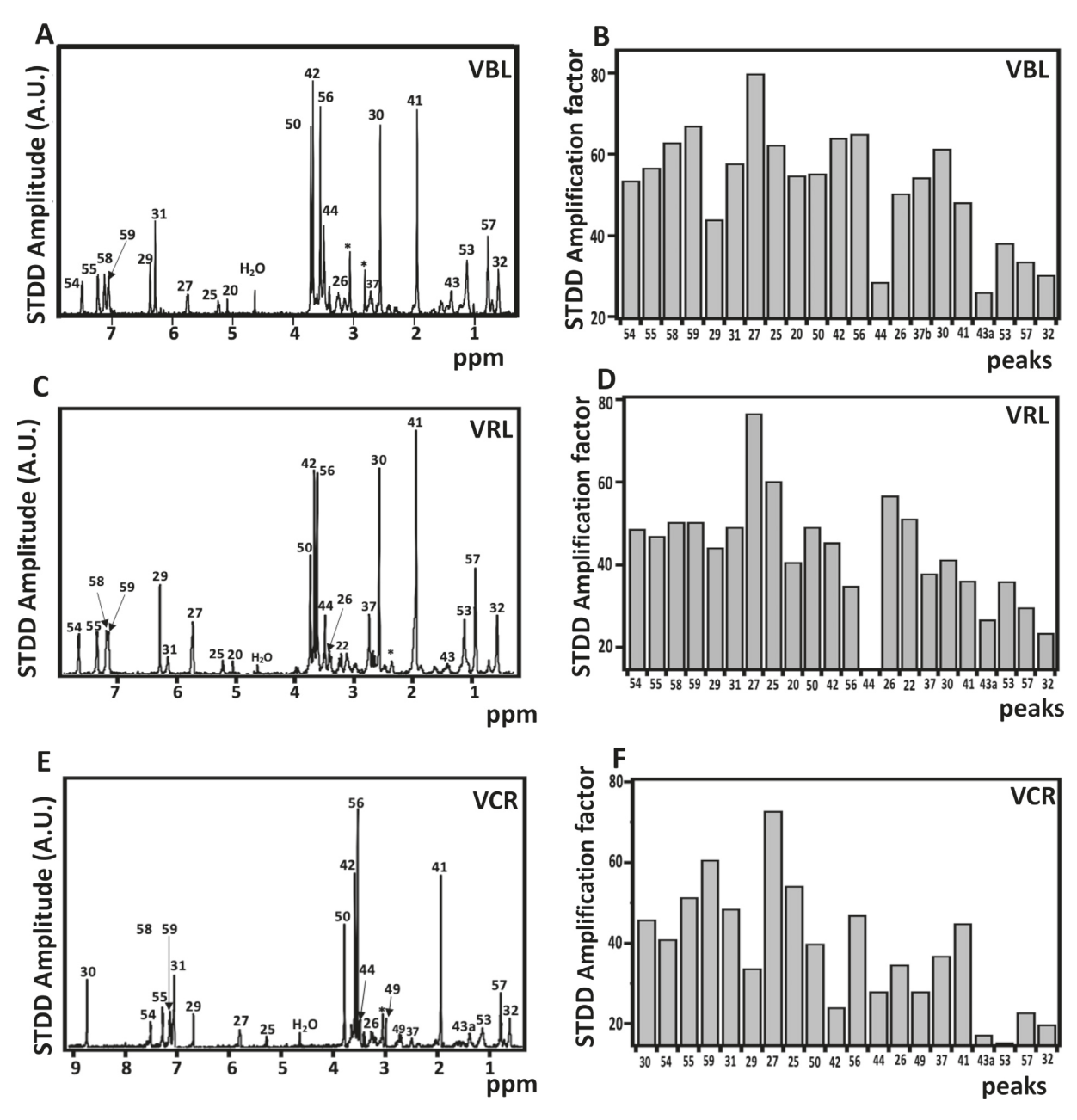


Fig. 5. The functional groups of vinca alkaloids involved in its interactions with Pgp investigated by STDD NMR technique. (A) (C), and (E) represent the ¹H 1D STDD NMR spectrum of VBL, VCR, and VRL, respectively. The category plots of STDD amplification factors deduced for (B) VBL, (D) VRL, and (F) VCR, respectively, were estimated from the ¹H 1D STDD NMR spectrum. The peak labels in each panel correspond to protons in Fig. 1. Sub-labels 'a' and 'b' represent axial and equatorial protons, respectively. The * represents unidentified peaks

are presented in panels 5B, 5D, and 5F, respectively. On average, VBL exhibited the highest STDD amplification factors per peak, followed by VRL. C_{27} notably displayed the highest amplification factor for the three drugs, indicating its potentially critical role in the interaction between VAs and Pgp. In addition, other protons from C_{56} , C_{27} , C_{59} , C_{25} , C_{30} , and C_{26} (Fig. 5; see Fig. 1) showed significant amplification amplitude for the Pgp-VAs interactions. Note that the STDD NMR experiments were limited by the concentration of the ligand that can be employed. At lower ligand concentrations, it was impossible to generate a sufficient signal-to-noise ratio for efficient STDD NMR analysis. This development limited the ability to characterize the functional groups involved in Pgp-VA binding into high-and low-affinity. For simplicity, the common functional groups on the VAs involving in its binding to Pgp are shown in Fig. S1.

Analysis of the impact of VBL, VRL, and VCR on the height distribution of Pgp determined by AFM imaging

The catalytic function of Pgp relies significantly on its conformational transition from an open-inward orientation (open towards the cytosolic region) to an open-outward orientation (open to the extracellular environment). AFM is a high-resolution imaging technique that has been used to explore ligand-induced conformational changes in Pgp. Ligands efficiently transported by the protein typically facilitate conformational changes that reposition the protein into an open-outward configuration. AFM imaging was employed to investigate drug-induced conformational shifts that might influence Pgp-mediated transport of the VAs. While techniques like X-ray crystallography and cryogenic Electron Microscopy (cryo-EM) have

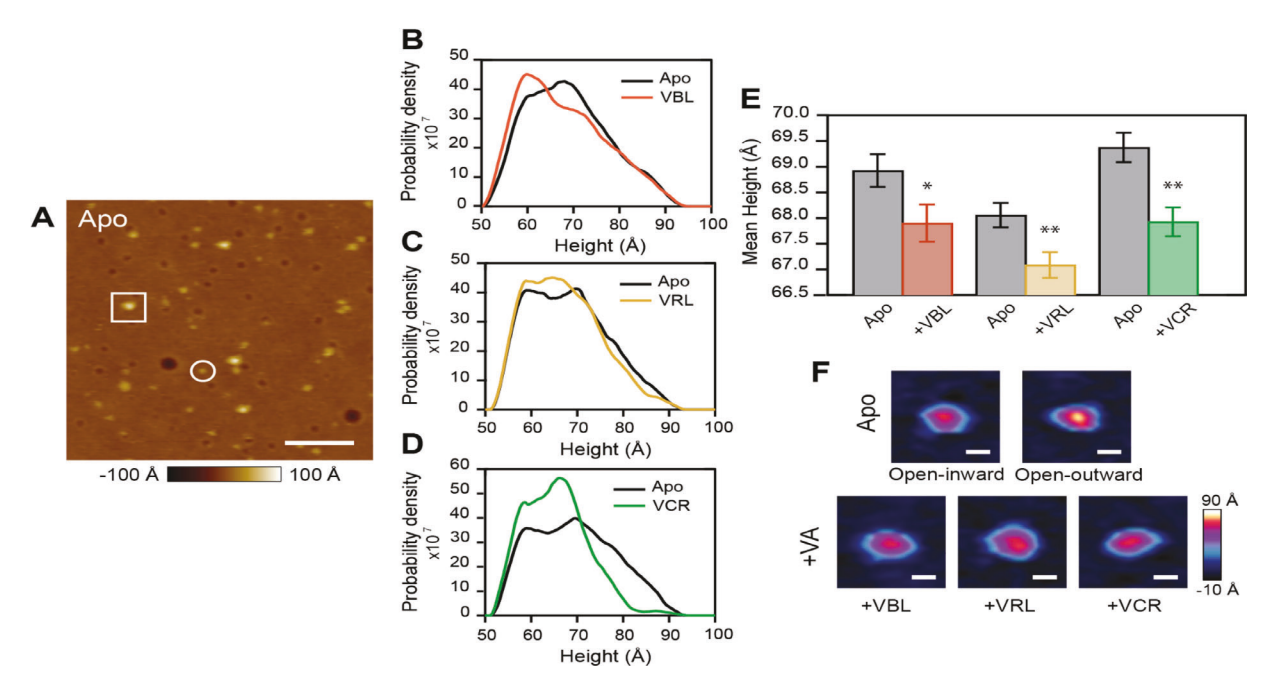


Fig. 6. The effect of vinca alkaloids on the height distributions of Pgp at the cytosolic domain (C-domain) deduced by AFM imaging. (A) A representative AFM image of apoPgp on glass demonstrates both C-side (boxed) and EC-side (circled) features; scale bar = 1000 Å. Smooth histograms illustrating the population shifts from apo (black) and in the presence of VBL (B; orange), VRL (C; gold), and VCR (D; green). The probability density shown on the y-axis was determined by integrating the histograms into unity area using SI units. (E) The mean heights of the C-side features are compared side-by-side to show relative shifts of drug-induced conformations from apoPgp; error bars are the standard error. The distributions were compared using a Student's T test and, following convention, * indicates p < 0.05 and ** indicates p < 0.01. (F) Following fitting with multiple Gaussian distributions using a model selection criterion (see Supplemental Information Fig. 1), features representative of the tallest (open-outward, $h \sim 80$ Å) and middle (open-inward, $h \sim 68$ Å) populations were selected for apoPgp (top row). In the presence of vinca alkaloids, the tallest population shifted downward to heights more typical of an open-inward state. Features with these heights are shown for VBL, VRL, and VCR; scale bars = 100 Å.

contributed significantly to our understanding of this protein, they rely on the average coordinates of atoms to determine the structures of biological molecules. ⁹⁰ In contrast, AFM imaging has the advantage of sampling through various conformations of a biological molecule, allowing the identification of conformational changes in individual molecules. ⁹¹

Fig. 6 provides insights into ligand-induced conformational changes in Pgp determined by AFM imaging. The identification of Cdomains and EC-domains within the lipid bilayer was achieved by measuring the particle heights as in previous work. 92 The C-side features were identified based on heights ranging from 55 to 90 Å. On the other hand, heights between 10 Å and 35 Å were attributed to ECside features (Fig. 6A). C-side-specific antibodies for Pgp have been employed in a previous study to ensure a robust differentiation of the C-side from the EC-side. 57 Smoothed histograms demonstrating height shifts in the C-side features of Pgp in the absence (Fig. 6B-D; black lines) and presence of saturating VBL (Fig. 6B), VRL (Fig. 6C), and VCR (Fig. 6D) are shown in Fig. 6. Analysis AFM imaging focused on C-side features due to the prominent conformational dynamics on that side of the protein compared to the E-side. To address potential batch-to-batch variations in the samples being imaged, we initiated the AFM imaging process by capturing images of Pgp without ligands. Subsequently, test compounds were introduced to the sample, and the imaging procedure was repeated. This approach also ensures that any observed shift in features occurs within a reasonably consistent distribution of Pgp protrusions. The AFM imaging data were analyzed using a comprehensive model selection criterion (See Supporting Information Fig. S1) and shifts in the tallest population were closely examined.

The sample size (N) of C-side features of apoPgp analyzed prior to the addition of VBL was 707, with the average height centered around 69 \pm 9 Å ($\pm\sigma$). The addition of 150 μ M of VBL (N=609) shifted the height distribution slightly to the left, with

the mean height reducing to 68 ± 9 Å (Fig. 6E, orange). Analysis of the C-side features was repeated for VRL and VCR. For VRL, apoPgp (N=1241) had a mean height of 68 ± 8 Å. Upon the addition 150 μ M VRL (N=984), a reduction in the average height of C-side features was noted, measuring 67 ± 8 Å (Fig. 6E, yellow). The number of C-side features of Pgp analyzed before and after adding VCR were 935 and 847, respectively. The introduction of 150 μ M VCR decreased the mean height from 69 ± 9 Å (apoPgp) to 68 ± 8 Å (Fig. 6E, green).

Discussion

The clinical application of some of the most pre-clinically potent chemotherapeutic agents is often limited by extreme non-target cytotoxicity. The action of Pgp, which pumps these drugs out of cells, necessitate the use of higher than necessary physiologically relevant dose, resulting in intolerable systemic toxicity. The use of Pgp inhibitors, concurrently with anticancer agents, has been touted but yielded little success.⁹³ Moreover, effectively inhibiting the function of Pgp may pose other serious health complications since the protein plays a crucial role in protecting susceptible tissues, such as those of the brain and testis. A better approach to efficient chemotherapy would involve the development of chemotherapeutic agents capable of overcoming Pgp-mediated efflux. A comprehensive understanding of the mechanisms underlying the differential transport of drugs, such as the VAs, is required to address this challenge. In this regard, a model aimed at elucidating the intricate process of Pgp-mediated transport of the VAs is presented in Fig. 7.

*In silico*³⁰ and biophysical data^{67,94} collectively suggest the existence of at least two distinct binding sites on the protein for the VAs: one characterized by high affinity and the other, low affinity. The high-affinity site is purportedly located closer to the outer leaflet of the membrane, within the conventional central cavity.^{30,95} The

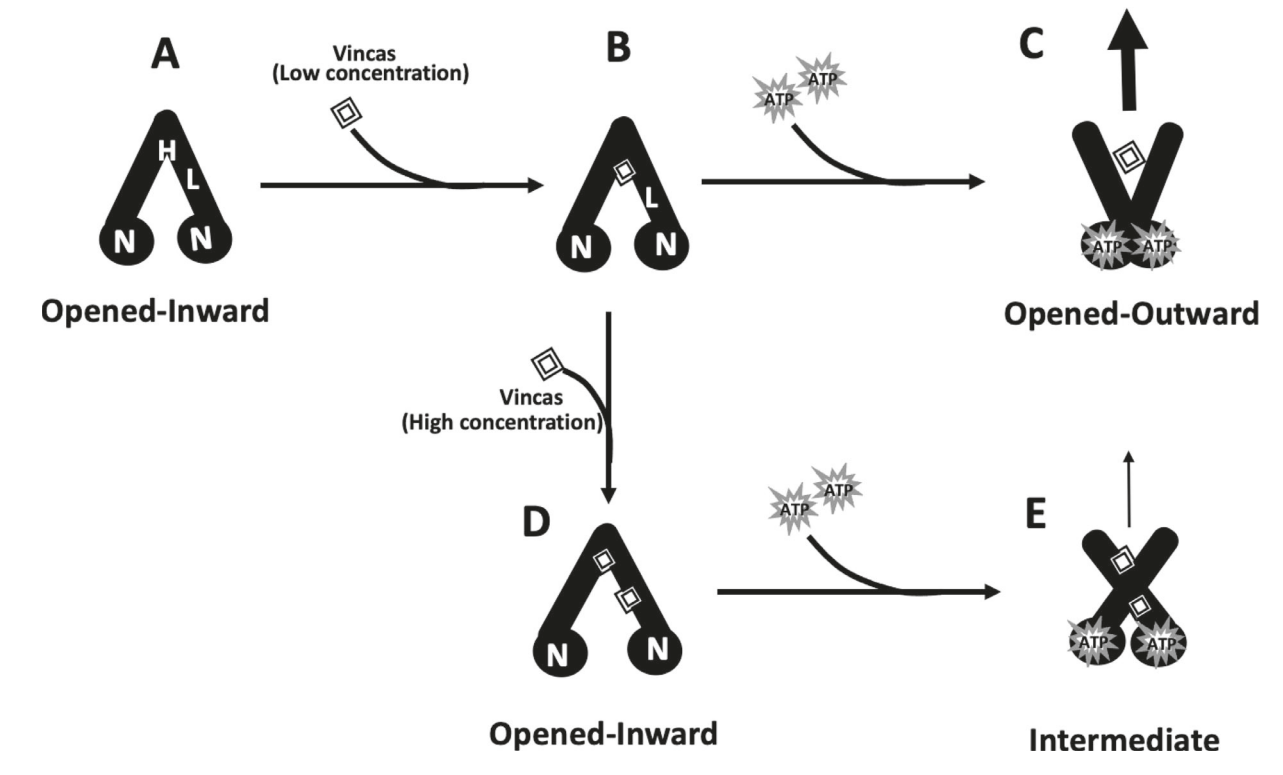


Fig. 7. Model illustrating VA-induced activation of Pgp-mediated ATP hydrolysis and transport. The figure illustrates cartoons of Pgp in the open-inward (A, B, D), opened outward (C), and intermediate (E) conformations. Pgp is represented in solid black, with the black circular region labeled 'N' representing the nucleotide-binding domain (NBD). Molecules of vinca alkaloids are shown as diamonds. H and L depict the proposed high-and low-affinity binding sites, respectively, of the vinca alkaloids on Pgp. The size of the vertical arrows reflects the degree of Pgp-mediated ATP hydrolysis and transport of the vinca alkaloids.

lower-affinity site is located on the surface of the protein around the protein-lipid interface, closer to the inner leaflet of the membrane.³⁰ We proposed that at low substrate concentrations, VAs bind to the high-affinity binding sites within the central cavity of the protein, stimulating ATP binding and hydrolysis (Fig. 7). The rate of ATPase activity induced by VBL at relatively lower concentration was approximately 2- and 9-fold higher compared to VRL and VCR, respectively (Fig. 2). Given that other previous reports indicate a direct interrelationship between the rate of Pgp-mediated ATP hydrolysis and transport for most substrates⁷⁰, we infer that among the three drugs tested, VBL is the most effectively transported by Pgp at lower drug concentrations. Applying the same analogy, VCR would be expected to be the least transported. This observation aligns with experimental data showing that the transport rates among the tested VAs are in the order VBL > VRL > VCR. 25,31,96 Pgp-mediated stimulation of ATPase activity and transport may typically be underpinned by two primary mechanisms: Pgp-ligand binding affinities and ligand-induced conformational changes in the protein. Binding studies employing ligand-induced quenching of tryptophan residues (Fig. 3) revealed that at low substrate concentrations, the affinity of VBL to Pgp is approximately 116% and 225% higher than that of VRL and VCR, respectively. These findings are further reinforced by the identification of groups in VAs potentially engaged in Pgp-VAs interactions. Protons linked to the C₃₀ moiety (Fig. 1 and Fig. 5), which characteristically distinguishes VBL from VCR, displayed notable but varying STDD amplification factors, with VBL exhibiting the highest level of STDD. Furthermore, a previously solved cryo-EM structure of VCRbound Pgp indicates the possibility of an aldehyde-amide condensation reaction involving C₃₀ moiety on the VAs.⁹⁵ A template-fit molecular docking⁹⁷ and subsequent analysis using LigPlus software⁹⁸ revealed similar interactions between C30 on VCR and glutamine residue 990 (Fig. S3F). This condensation reaction may have contributed significantly to the disparities observed in the differential

affinity of the VAs to Pgp. On the contrary, no such interaction was observed for VCR at the low-affinity site. As noted in Fig. S3, the interactions between the VAs and Pgp at both the high-and-low affinity sites were predominantly hydrophobic, with methyl groups showing significant hydrophobic interactions with Pgp residues. Notably, VBL exhibited relatively higher number of hydrophobic interactions with Pgp residues, consistent with our experimental data. Unfortunately, besides the methyl groups of the VAs that consistently showed similar hydrophobic interactions with Pgp, all other forms of non-hydrophobic bonding appear ligand-specific. This development made it difficult to hone in on the polar functional groups on VAs involved in Pgp-VA binding at the high-and-low affinity sites without being ligand specific.

Surprisingly, conformational studies (Fig. 4) showed that the VAs have no significant impact on Pgp conformation at low substrate concentrations (10 μ M). This finding was unexpected, as most Pgp substrates typically induce notable shifts in the protein's conformation.^{46,99} However, it is likely the concentration used (10 μ M) might not have been sufficient to saturate the high-affinity binding site and induce observable conformational changes. An earlier study that employed hydrogen-deuterium exchange mass spectrometry also reported similar observations for VBL. 100 Based on our data and previously reported studies^{30,95,100}, it appears that at the concentrations tested (10 μ M), differences in ligand-induced conformational changes in the protein may not be the bottle-neck for transport. Instead, the differential binding affinity likely serves as the ratelimiting mechanism governing the transport of VAs by Pgp. Note that these results do not rule out the possibility of ligand-induced changes in the conformational dynamics of individual peptide segments that facilitate the coupling between the drug binding sites and the NBDs. While such changes may not be readily detectable using the techniques employed in this study, they could still be significant enough to stimulate transport. For instance, although the binding of VBL^{101,102}

and VCR⁹⁵ to Pgp did not result in significant structural differences in the overall protein structure compared to the drug-free state, alterations in the structure of transmembrane helix 12 (TM12) were observed upon binding.⁹⁵ These alterations are expected as TM12 plays a pivotal role in mediating communication between the central drug-binding cavity and NBDs.¹⁰³

Interestingly, at higher drug concentrations, the VAs seem to occupy the low-affinity site, purportedly located at the interface between the protein and the lipid bilayer.³⁰ At these higher drug concentrations, the ATPase activity induced by the VAs were inhibitory (Fig. 2). Two available theories can explain the observed inhibition of ATPase activity by the VAs. Firstly, numerous studies have linked the traditionally elevated basal ATPase activity of Pgp to the presence of endogenous substances, such as cholesterol, within the lipid bilayer. 104 Although not transported by Pgp 105, these endogenous lipids may be flip-flopped between the lipid bilayer leaflets. 106,107 A ligand, interacting with the same binding sites as these endogenous substrates but at a slower rate, may appear to inhibit the rate of ATPase activity since the observed Pgp-mediated ATPase activity encompasses both the basal and ligand-induced activation. This line of reasoning is supported by the suggested location of the inhibitory binding sites of the VAs³⁰ and the notion that Pgp-mediated ATPase activity depends on a complex interplay between ligands, the membrane environment, and the protein itself. 108 The second theory posits that VAs exhibit behaviors akin to certain inhibitors such as tariguidar and verapamil. These inhibitors act as substrates at low concentrations and inhibitors at higher concentrations.⁹⁵ The latter theory, among the two proposed, is the most substantiated by the available literature. When the VAs bind to the second site, they likely impede the necessary protein reorientation required for substrate transport. However, unlike potent inhibitors, the VAs exhibit relatively lower affinity for the second binding site (Fig. 3), making them unlikely candidates as potent Pgp inhibitors. Studies have revealed that the second binding site is surrounded by multiple transmembrane helices (TM4, TM10, TM9, and TM12).⁹⁵ Additionally, the surface of the inhibitory/second binding site features several phenylalanine residues that interact with the bound ligand 30,95, suggesting that the binding of the VAs at this site may heavily depend on weak hydrophobic interactions. The binding of Pgp inhibitors to the inhibitory binding sites on Pgp appears to restrict TM9 and TM10⁹⁵, the two transmembrane helices known to prevent substrate translocation. 109,110 The inhibitory site is also believed to obstruct the access tunnel and vestibule of the protein, preventing the necessary shift when a substrate binds to the central binding cavity. 95 The K_i values extracted from the ATPase kinetic curves for VAs (Fig. 2) suggest that VCR has the highest inhibitory potential at higher substrate concentration, followed by VRL and VBL. In addition, the order of affinity to Pgp at the inhibitory binding site, $K_{D \cdot L}$, is a reverse of the stimulatory binding site (Fig. 3, Table S2). VCR exhibited the highest binding affinity at the inhibitory site, followed by VRL.

Even though there were some differences in the Pgp conformational changes induced by the VAs at 150 μ M, these changes were not substantial. These observations concur with the AFM imaging results, which assessed changes in the height distributions Pgp protrusion within the cytosolic region when exposed to 150 μ M VAs (Fig. 6). VBL (Fig. 6B) and VRL (Fig. 6C) had minimal impact (\sim 1 Å) on the average C-side height. VCR (Fig. 6D) shifted the distribution the most, though still a modest 1.4 Å difference in the means. This indicates a greater increase in the number of C-side features with heights corresponding to wide open-inward conformations, which is associated with shorter C-side protrusion. Studies have shown that the activation of Pgp-mediated transport is often dependent on ligand-induced conformational changes in Pgp. 46,99 Pgp-mediated transport would be minimal when the protein is in a predominantly wide opened inward conformation. 57 Based on these results, we can infer

that, compared to the other two tested drugs, VCR exerts the highest inhibitory influence on Pgp-mediated transport under saturating substrate concentrations. The inhibitory potential is evident from the ability of VCR to shift the protein's conformation, resulting in a 1.33-fold increase in the widely open-inward conformation relative to the apo condition (Fig. 6 & Fig. S1). This is a slightly larger effect compared to that of VBL and VRL, which increased open-inward conformations 1.28-fold and 1.23-fold, respectively. The subtle conformational changes detected via the sensitive AFM probe may be associated with the underlying structural mechanism mediating the transport of VAs by Pgp.

Remarkably, when AMPPNP was present, VAs at low concentrations (10 μ M) induced a conformational shift in Pgp similar to saturating AMPPNP alone (Fig. 4), indicating an open-outward conformation. This similarity in conformational changes may be attributed to the low substrate concentration used in comparison to the saturating concentration of AMPPNP. At both saturating drug (150 μ M) and AMPPNP (3.2 mM) concentrations, the VAs induced a shift in Pgp conformation that is intermediate between open-inward and open-outward (Fig. 4). However, the conformational shift induced by saturating VCR (Fig. 4H) in the presence of AMPPNP was lesser than those observed for VBL (Fig. 4D) and VRL (Fig. 4F). On the contrary, there was no significant difference observed between the effects of VBL (Fig. 4D) and VRL (Fig. 4F).

There is a demand for the next generation of VAs with increased response rates and manageable toxicity. The development of vinflunine, a third-generation vinca alkaloid with lower toxicity, is promising. 111 Unfortunately, vinflunine is less potent and requires at least a 17-fold higher concentration for a similar effect as VCR. 112 Secondly, the development of new derivatives has been laborious with little success. Identification of functional groups involved in Pgp-VAs interactions may offer new hope for a rational drug design. The STDD NMR revealed that comparable groups on the VAs are involved in Pgp interactions. Peaks from proton linked to C₂₇ on the indoline group of the VAs (see Fig. 1 and Fig. 5) showed the highest interaction with the protein. In addition, the methyl groups appear to be highly involved in drug-Pgp interactions, as shown by the significant 1D ¹H STDD NMR signals from C_{30} , C_{41} , C_{42} , C_{50} , C_{56} , and C_{57} . Perhaps this explains why substituting a methyl group on VBL (see Fig.1; N_{11}) with an aldehyde (VCR) resulted in disparate Pgp-mediated efflux rates between the two drugs. VBL showed the highest average STDD amplification factor, which supports our drug-protein affinity data (Fig. 3). Reducing hydrogen bond acceptor (HBA) groups 113 at regions implicated in Pgp-drug recognition revealed by the STDD NMR analysis (Fig. 5) could potentially lead to the development of next-generation VAs capable of evading the transporter. For instance, altering specific methyl functional residues (C30, C41, C42, C50, C56, and C57) in the VAs that exhibited notable STDD NMR amplification factors could lead to the development of novel derivatives of VAs with either a reduced affinity or enhanced ability to evade the activity of the transporter. This development would enhance cellular accumulation and improve the effectiveness of the VA as chemotherapeutic agents. While this approach holds promise for the development of improved derivatives, a limitation lies in the potential loss of functionality. This bottleneck could be adrressed by coupling our understanding of the functional groups responsible for the binding of the VAs to Pgp with available structure-activity relationship (SAR) studies for the VAs and microtubules 114,115, potentially guiding us in our search for more effective next-generation vinca alkaloid derivatives.

Fig. 7 illustrates a model, derived from the summary of our data and existing literature, that depicts a probable mechanism for Pgpmediated transport of VAs. At low substrate concentrations, VAs bind to the stimulatory binding site located within the central cavity of the protein. During this phase, no significant conformational change takes place. However, subtle alterations in TM 12 promote ATP

binding at the NBDs, causing the protein to shift into an open-outward conformation, thus facilitating transport (Fig. 7A ->7B ->7C). However, at high substrate concentrations, VAs occupy both the stimulatory and inhibitory binding sites on Pgp. With both binding sites engaged, ATP binding induces an intermediate conformational state between open-inward and open-outward (Fig. 7A ->7B->7D ->7E). This intermediate conformation inhibits Pgp-mediated ATP hydrolysis and transport. The model presented in this study may be extrapolated to account for Pgp-mediated transport of substrates with at least known Pgp-coupled ATPase kinetic data.

In summary, our findings elucidate a probable structural mechanism governing the Pgp-mediated efflux of VAs. We have also identified the potential functional groups on VAs involved in substrate recognition and binding to Pgp. These findings, coupled with SAR studies involving VAs and microtubules, could lay the foundation for rational drug design aimed at the next-generation VAs that show higher efficacy and less systemic toxicity.

Author contributions

GAKM: Conceptualization, formal analysis, investigation, methodology, writing — original draft, writing — review & editing; KGS: formal analysis, methodology, visualization, writing — review & editing; MGB: writing — review & editing; AGR: conceptualization, supervision, funding acquisition; GMK: conceptualization, supervision, funding acquisition, writing — review & editing.

Data availability Statement

Data is available upon request.

Declaration of competing interest

The authors declare that they have no known competing financial interests or personal relationships that could have appeared to influence the work reported in this paper.

Funding

This work was supported in part by the National Institutes of Health (1R01CA204846-01A1, to A.G.R.) and the National Science Foundation (2122027, to G.M.K.). K.G.S. acknowledges support from the Research Excellence Program (REP) at the University of Missouri.

Supplementary materials

Supplementary material associated with this article can be found in the online version at doi:10.1016/j.xphs.2024.03.014.

Reference

- Wang J, Seebacher N, Shi H, Kan Q, Duan Z. Novel strategies to prevent the development of multidrug resistance (MDR) in cancer. *Oncotarget*. 2017;8(48):84559– 84571. https://doi.org/10.18632/oncotarget.19187.
- Longley DB, Johnston PG. Molecular mechanisms of drug resistance. J Pathol. 2005;205(2):275–292. https://doi.org/10.1002/path.1706.
- Zhang J, Sun T, Liang L, Wu T, Wang Q. Drug promiscuity of P-glycoprotein and its mechanism of interaction with paclitaxel and doxorubicin. Soft Matter. 2013;10 (3):438–445. https://doi.org/10.1039/C3SM52499J.
- Boumendjel A, Boutonnat J, Robert J. ABC Transporters and Multidrug Resistance. John Wiley & Sons; 2009.
- Robinson K, Tiriveedhi V. Perplexing role of P-glycoprotein in tumor microenvironment. Front Oncol. 2020;10. https://doi.org/10.3389/fonc.2020.00265.
- Katayama K, Noguchi K, Sugimoto Y. Regulations of P-Glycoprotein/ABCB1/MDR1 in Human Cancer Cells. New J Sci. 2014. https://doi.org/10.1155/2014/476974. Published online.
- 7. Nanayakkara AK, Follit CA, Chen G, Williams NS, Vogel PD, Wise JG. Targeted inhibitors of P-glycoprotein increase chemotherapeutic-induced mortality of

- multidrug resistant tumor cells. Sci Rep. 2018;8(1):967. https://doi.org/10.1038/s41598-018-19325-x
- Noack A, Noack S, Buettner M, Naim HY, Löscher W. Intercellular transfer of P-gly-coprotein in human blood-brain barrier endothelial cells is increased by histone deacetylase inhibitors. Sci Rep. 2016;6(1):29253. https://doi.org/10.1038/srep.29253.
- Pokharel D, Roseblade A, Oenarto V, Lu JF, Bebawy M. Proteins regulating the intercellular transfer and function of P-glycoprotein in multidrug-resistant cancer. 10.3332/ecancer.2017.768.
- MdL Amin. P-glycoprotein inhibition for optimal drug delivery. Drug Target Insights. 2013;7:27–34. https://doi.org/10.4137/DTI.S12519.
- Callaghan R, Luk F, Bebawy M. Inhibition of the multidrug resistance P-glycoprotein: Time for a change of strategy? *Drug Metab Dispos*. 2014;42(4):623–631. https://doi.org/10.1124/dmd.113.056176.
- Waghray D, Zhang Q. Inhibit or evade multidrug resistance P-glycoprotein in cancer treatment. J Med Chem. 2017;61(12):5108–5121. https://doi.org/10.1021/acs.imedchem.7b01457.
- 13. Keogh JP, Kunta JR. Development, validation and utility of an in vitro technique for assessment of potential clinical drug-drug interactions involving P-glycoprotein. Eur J Pharm Sci. 2006;27(5):543–554. https://doi.org/10.1016/j.ejps.2005.11.011.
- van Der Heijden R, Jacobs DI, Snoeijer W, Hallard D, Verpoorte R. The Catharanthus alkaloids: pharmacognosy and biotechnology. *Curr Med Chem.* 2004;11 (5):607–628. https://doi.org/10.2174/0929867043455846.
- Tyagi G, Jangir DK, Singh P, Mehrotra R. DNA interaction studies of an anticancer plant alkaloid, vincristine, using Fourier transform infrared spectroscopy. DNA Cell Biol. 2010;29(11):693–699. https://doi.org/10.1089/dna.2010.1035.
- Mhaidat N, Alzoubi K, Khabour O, et al. Assessment of genotoxicity of vincristine, vinblastine and vinorelbine in human cultured lymphocytes: a comparative study. Balkan J Med Genet. 2016;19(1):13–20. https://doi.org/10.1515/bjmg-2016-0002.
- Moudi M, Go R, Yien CYS, Mohd Nazre. Vinca alkaloids. Int J Prev Med. 2013;4 (11):1231–1235.
- Vardanyan RS, Hruby VJ. 30 antineoplastics. In: Vardanyan RS, Hruby VJ, eds. Synthesis of Essential Drugs. Elsevier; 2006;389–418. https://doi.org/10.1016/ B978-044452166-8/50030-3.
- Dhyani P, Quispe C, Sharma E, et al. Anticancer potential of alkaloids: a key emphasis to colchicine, vinblastine, vincristine, vindesine, vinorelbine and vincamine. Cancer Cell Int. 2022;22(1):206. https://doi.org/10.1186/s12935-022-02624-9.
- Duffin J. Poisoning the spindle: serendipity and discovery of the anti-tumor properties of the Vinca alkaloids. *Can Bull Med Hist*. 2000;17(1-2):155–192. https://doi.org/10.3138/cbmh.17.1.155.
- Ngan VK, Bellman K, Panda D, Hill BT, Jordan MA, Wilson L. Novel Actions of the Antitumor Drugs Vinflunine and Vinorelbine on Microtubules. Cancer Res. 2000;60(18):5045–5051.
- Lobert S, Vulevic B, Correia JJ. Interaction of vinca alkaloids with tubulin: a comparison of vinblastine, vincristine, and vinorelbine. *Biochemistry*. 1996;35 (21):6806–6814. https://doi.org/10.1021/bi953037i.
- Kruczynski A, Barret JM, Etiévant C, Colpaert F, Fahy J, Hill BT. Antimitotic and tubulin-interacting properties of vinflunine, a novel fluorinated Vinca alkaloid. Biochem Pharmacol. 1998;55(5):635–648. https://doi.org/10.1016/S0006-2952 (97)00505-4.
- Wishart DS, Feunang YD, Guo AC, et al. DrugBank 5.0: a major update to the Drug-Bank database for 2018. Nucleic Acids Res. 2018;46(D1):D1074–D1082. https:// doi.org/10.1093/nar/gkx1037.
- Ferguson PJ, Cass CE. Differential cellular retention of vincristine and vinblastine by cultured human promyelocytic leukemia HL-60/Cl cells: the basis of differential toxicity. Cancer Res. 1985;45(11):5480–5488. Part 1.
- Rivera-Fillat MP, Pallarés-Trujillo J, Domènech C, Grau-Oliete MR. Comparative uptake, retention and action of vincristine, vinblastine and vindesine on murine leukaemic lymphoblasts sensitive and resistant to vincristine. Br J Pharmacol. 1988;93(4):902–908
- 27. Krikorian A, Breillout F. Vinorelbine (Navelbine). A new semisynthetic vinca alkaloid. *Onkologie*. 1991;14(1):7–12. https://doi.org/10.1159/000216938.
- Gout PW, Noble RL, Bruchovsky N, Beer CT. Vinblastine and vincristine—growthinhibitory effects correlate with their retention by cultured Nb 2 node lymphoma cells. Int J Cancer. 1984;34(2):245–248. https://doi.org/10.1002/ijc.2910340216.
- 29. Barthomeuf C, Grassi J, Demeule M, Fournier C, Boivin D, Béliveau R. Inhibition of P-glycoprotein transport function and reversion of MDR1 multidrug resistance by cnidiadin. *Cancer Chemother Pharmacol.* 2005;56(2):173–181. https://doi.org/10.1007/s00280-004-0914-y.
- 30. Iqbal S, Flux C, Briggs DA, et al. Vinca alkaloid binding to P-glycoprotein occurs in a processive manner. *Biochimica et Biophysica Acta (BBA) Biomembranes*. 2022;1864(10): 184005. https://doi.org/10.1016/j.bbamem.2022.184005.
- Lin X, Skolnik S, Chen X, Wang J. Attenuation of intestinal absorption by major efflux transporters: quantitative tools and strategies using a Caco-2 model. *Drug Metab Dispos*. 2011;39(2):265–274. https://doi.org/10.1124/ dmd.110.034629.
- Lerner-Marmarosh N, Gimi K, Urbatsch IL, Gros P, Senior AE. Large scale purification of detergent-soluble P-glycoprotein from Pichia pastoris cells and characterization of nucleotide binding properties of wild-type, walker A, and walker B mutant proteins. J Biol Chem. 1999;274:34711–34718. https://doi.org/10.1074/jbc.274.49.34711.

- Urbatsch IL, Beaudet L, Carrier I, Gros P. Mutations in either nucleotide-binding site of P-glycoprotein (Mdr3) prevent vanadate trapping of nucleotide at both sites. *Biochemistry*. 1998;37(13):4592–4602. https://doi.org/10.1021/ bi9728001.
- Ledwitch KV, Barnes RW, Roberts AG. Unravelling the complex drug-drug interactions of the cardiovascular drugs, verapamil and digoxin, with P-glycoprotein. *Biosci Rep.* 2016;36(2):1–14. https://doi.org/10.1042/BSR20150317.
- Rao US, Nuti SL. Identification of two different states of p-glycoprotein in its catalytic cycle: role of the linker region in the transition between these two states*. J Biol Chem. 2003;278(47):46576–46582. https://doi.org/10.1074/jbc.M308078200.
- Chifflet S, Torriglia A, Chiesa R, Tolosa S. A method for the determination of inorganic phosphate in the presence of labile organic phosphate and high concentrations of protein: application to lens ATPases. Anal Biochem. 1988;168(1):1–4. https://doi.org/10.1016/0003-2697(88)90002-4.
- Mensah GAK, Schaefer KG, Bartlett MG, Roberts AG, King GM. Drug-induced conformational dynamics of P-glycoprotein underlies the transport of camptothecin analogs. Int J Mol Sci. 2023;24(22):16058. https://doi.org/10.3390/ijms242216058.
- Nguyen PH, Sigdel KP, Schaefer KG, Mensah GAK, King GM, Roberts AG. The effects of anthracycline drugs on the conformational distribution of mouse P-glycoprotein explains their transport rate differences. *Biochem Pharmacol*. 2020;174: 113813. https://doi.org/10.1016/j.bcp.2020.113813.
- Yammine A, Gao J, Kwan AH. Tryptophan fluorescence quenching assays for measuring protein-ligand binding affinities: principles and a practical guide. *Bio Protoc.* 2019;9(11):e3253. https://doi.org/10.21769/BioProtoc.3253.
- Sharom FJ, Russell PL, Qu Q, Lu P. Fluorescence techniques for studying membrane transport proteins: the P-glycoprotein multidrug transporter. *Methods Mol Biol.* 2003;227:109–128. https://doi.org/10.1385/1-59259-387-9:109.
- 41. Lakowicz JR. Principles of Fluorescence Spectroscopy. Springer; 2011. 3rd edition.
- Jeewantha HA, Ivanovich SA, Mihailovich KP. Validated spectrophotometric method for the estimation of vincristine and vinblastine. *Int J Pharmacy Pharma*ceut Sci. 2017:78–86. https://doi.org/10.22159/ijpps.2017v9i4.16577. Published online April 1.
- Reddy CMB, Reddy GVS. Validated method for vinblastin by spectrophotometry in bulk drug and pharmaceutical formulations. Published online 2012:5.
- 44. Cioni P, Strambini GB. Acrylamide quenching of protein phosphorescence as a monitor of structural fluctuations in the globular fold. *J Am Chem Soc.* 1998;120 (45):11749–11757. https://doi.org/10.1021/ja9820543.
- Russell PL, Sharom FJ. Conformational and functional characterization of trapped complexes of the P-glycoprotein multidrug transporter. *Biochem J.* 2006; 399:315–323. https://doi.org/10.1042/BJ20060015.
- Zoghbi ME, Mok L, Swartz DJ, et al. Substrate-induced conformational changes in the nucleotide-binding domains of lipid bilayer-associated P-glycoprotein during ATP hydrolysis. J Biol Chem. 2017. https://doi.org/10.1074/jbc.M117.814186. Published online October 9.
- Viegas A, Manso J, Nobrega FL, Cabrita EJ. Saturation-transfer difference (STD) NMR: a simple and fast method for ligand screening and characterization of protein binding. J Chem Educ. 2011;88(7):990–994. https://doi.org/10.1021/ed101169t.
- Roberts AG, Sjogren SE, Fomina N, Vu KT, Almutairi A, Halpert JR. NMR-derived models of amidopyrine and its metabolites in complexes with rabbit cytochrome P450 2B4 reveal a structural mechanism of sequential N-dealkylation. *Biochemistry*. 2011:50:2123–2134. https://doi.org/10.1021/bi101797v.
- Xu YD, Lai RY, Procházková E, Stenzel MH. Saturation transfer difference NMR spectroscopy for the elucidation of supramolecular albumin—polymer interactions. ACS Macro Lett. 2021;10(7):819–824. https://doi.org/10.1021/acsmacrolett.1c00270.
- 50. Claasen B, Axmann M, Meinecke R, Meyer B. Direct observation of ligand binding to membrane proteins in living cells by a saturation transfer double difference (STDD) NMR spectroscopy method shows a significantly higher affinity of integrin αIIbβ3 in native platelets than in liposomes. J Am Chem Soc. 2005;127:916–919.
- Haselhorst T, Munster-Kuhnel AK, Oschlies M, Tiralongo J, Gerardy-Schahn R, von Itzstein M. Direct detection of ligand binding to Sepharose-immobilised protein using saturation transfer double difference (STDD) NMR spectroscopy. *Biochem Biophys Res Commun*. 2007;359:866–870. https://doi.org/10.1016/j.bbrc.2007.05.204.
- Venkitakrishnan RP, Benard O, Max M, Markley JL, FM Assadi-Porter. Use of NMR saturation transfer difference spectroscopy to study ligand binding to membrane proteins. Membrane Protein Struct Dynamics: Methods Protocols. 2012:47–63. Published online.
- Liu ML, Mao XA, Ye CH, Huang H, Nicholson JK, Lindon JC. Improved WATERGATE pulse sequences for solvent suppression in NMR spectroscopy. J Magn Reson. 1998;132:125–129. https://doi.org/10.1006/jmre.1998.1405.
- 54. Mayer M, Meyer B. Group epitope mapping by saturation transfer difference NMR to identify segments of a ligand in direct contact with a protein receptor. *J Am Chem Soc.* 2001;123:6108–6117.
- Müller DJ, Dumitru AC, Lo Giudice C, et al. Atomic force microscopy-based force spectroscopy and multiparametric imaging of biomolecular and cellular systems. *Chem Rev.* 2021;121(19):11701–11725. https://doi.org/10.1021/acs.chemrev.0c00617.
- Vahabi S, Nazemi Salman B, Javanmard A. Atomic force microscopy application in biological research: a review study. *Iran J Med Sci.* 2013;38(2):76–83.
- Sigdel KP, Wilt LA, Marsh BP, Roberts AG, King GM. The conformation and dynamics of P-glycoprotein in a lipid bilayer investigated by atomic force microscopy. *Biochem Pharmacol.* 2018;156:302–311. https://doi.org/10.1016/j.bcp.2018.08.017.
- Chu CY, Henderson DJ, Parmeter CF. On discrete Epanechnikov kernel functions. *Comput Stat Data Anal.* 2017;116:79–105. https://doi.org/10.1016/j.csda.2017.07. 003.

- Sauna ZE, Ambudkar SV. About a switch: how P-glycoprotein (ABCB1) harnesses the energy of ATP binding and hydrolysis to do mechanical work. Mol Cancer Ther. 2007;6(1):13–23. https://doi.org/10.1158/1535-7163.MCT-06-0155.
- Sharom FJ. The P-glycoprotein multidrug transporter. Essays Biochem. 2011;50:161–178. https://doi.org/10.1042/bse0500161.
- 61. Shalinsky DR, Jekunen AP, Alcaraz JE, et al. Regulation of initial vinblastine influx by P-glycoprotein. *Br J Cancer*. 1993;67(1):30–36. https://doi.org/10.1038/bjc.1993.6.
- Wilt LA, Nguyen D, Roberts AG. Insights into the molecular mechanism of triptan transport by P-glycoprotein. J Pharm Sci. 2017;106:1670–1679. https://doi.org/ 10.1016/j.xphs.2017.02.032.
- Garrigos M, Mir LM, Orlowski S. Competitive and non-competitive inhibition of the multidrug-resistance-associated P-glycoprotein ATPase-further experimental evidence for a multisite model. Eur J Biochem / FEBS. 1997;244(2):664–673.
- Martin C, Higgins CF, Callaghan R. The vinblastine binding site adopts high- and low-affinity conformations during a transport cycle of P-glycoprotein. *Biochemistry*. 2001;40(51):15733–15742.
- Safa AR. Identification and characterization of the binding sites of P-glycoprotein for multidrug resistance-related drugs and modulators. Curr Med Chem Anticancer Agents. 2004;4(1):1–17.
- Tamai I, Safa AR. Competitive interaction of cyclosporins with the Vinca alkaloidbinding site of P-glycoprotein in multidrug-resistant cells. *J Biol Chem.* 1990;265 (27):16509–16513.
- Aanismaa P, Seelig A. P-Glycoprotein kinetics measured in plasma membrane vesicles and living cells. *Biochemistry*. 2007;46(11):3394–3404. https://doi.org/ 10.1021/bi0619526.
- Sharom FJ, Yu X, Chu JW, Doige CA. Characterization of the ATPase activity of Pglycoprotein from multidrug-resistant Chinese hamster ovary cells. *Biochem J.* 1995;308(2):381–390. https://doi.org/10.1042/bj3080381. Pt.
- Cisternino S, Rousselle C, Debray M, Scherrmann JM. In situ transport of vinblastine and selected P-glycoprotein substrates: implications for drug-drug interactions at the mouse blood-brain barrier. *Pharm Res.* 2004;21(8):1382–1389.
- Ambudkar SV, CO Cardarelli, Pashinsky I, Stein WD. Relation between the turnover number for vinblastine transport and for vinblastine-stimulated ATP hydrolysis by human P-glycoprotein. J Biol Chem. 1997;272(34):21160–21166. https:// doi.org/10.1074/jbc.272.34.21160.
- Young SD, Whissell M, Noble JCS, Cano PO, Lopez PG, Germond CJ. Phase II clinical trial results involving treatment with low-dose daily oral cyclophosphamide, weekly vinblastine, and rofecoxib in patients with advanced solid tumors. *Clinical Cancer Res.* 2006;12(10):3092–3098. https://doi.org/10.1158/1078-0432.CCR-05-2255.
- Gayer AV, Yakimov BP, Budylin GS, Shirshin EA. Evaluating the number of ligand binding sites on protein from tryptophan fluorescence quenching under typical experimental conditions. *J Biomed Photonics Eng.* 2020;6(2): 020303. https://doi. org/10.18287/JBPE20.06.020303.
- Sharom FJ, Liu R, Romsicki Y, Lu P. Insights into the structure and substrate interactions of the P-glycoprotein multidrug transporter from spectroscopic studies. *Biochim Biophys Acta*. 1999;1461(2):327–345.
- Ward A, Reyes CL, Yu J, Roth CB, Chang G. Flexibility in the ABC transporter MsbA: alternating access with a twist. PNAS. 2007;104(48):19005–19010. https://doi. org/10.1073/pnas.0709388104.
- Akbar SMD, Sreeramulu K, Sharma HC. Tryptophan fluorescence quenching as a binding assay to monitor protein conformation changes in the membrane of intact mitochondria. *J Bioenerg Biomembr*. 2016;48(3):241–247. https://doi.org/ 10.1007/s10863-016-9653-0.
- Gibbs ME, Wilt LA, Ledwitch KV, Roberts AG. A conformationally-gated model of methadone and loperamide transport by P-glycoprotein. J Pharm Sci. 2018. https://doi.org/10.1016/j.xphs.2018.02.019. Published online February 28.
- Jazaj D, Ghadami SA, Bemporad F, Chiti F. Probing conformational changes of monomeric transthyretin with second derivative fluorescence. Sci Rep. 2019;9 (1):10988. https://doi.org/10.1038/s41598-019-47230-4.
- Strambini GB, Gonnelli M. Fluorescence quenching of buried trp residues by acrylamide does not require penetration of the protein fold. J Phys Chem B. 2010;114(2):1089–1093. https://doi.org/10.1021/jp909567q.
- Swartz DJ, Singh A, Sok N, Thomas JN, Weber J, Urbatsch IL. Replacing the eleven native tryptophans by directed evolution produces an active P-glycoprotein with site-specific, non-conservative substitutions. *Sci Rep.* 2020;10(1):3224. https:// doi.org/10.1038/s41598-020-59802-w.
- Li J, Jaimes KF, Aller SG. Refined structures of mouse P-glycoprotein. Protein Sci. Publicat Protein Soc. 2014;23:34–46. https://doi.org/10.1002/pro.2387.
- Esser L, Zhou F, Pluchino KM, et al. Structures of the multidrug transporter p-glycoprotein reveal asymmetric ATP binding and the mechanism of polyspecificity ◆. J Biol Chem. 2017;292(2):446–461. https://doi.org/10.1074/jbc.M116.755884.
- Kim Y, Chen J. Molecular structure of human P-glycoprotein in the ATP-bound, outward-facing conformation. *Science* (1979). 2018;359(6378):915–919. https://doi.org/10.1126/science.aar7389.
- Moeller A, Lee SC, Tao H, et al. Distinct conformational spectrum of homologous multidrug ABC transporters. Structure. 2015;23(3):450–460. https://doi.org/ 10.1016/j.str.2014.12.013.
- Walpole S, Monaco S, Nepravishta R, Angulo J. Chapter twelve STD NMR as a technique for ligand screening and structural studies. In: Wand AJ, ed. *Methods in Enzymology*. Academic Press; 2019:423–451. https://doi.org/10.1016/bs.mie. 2018.08.018. Vol 615Biological NMR Part B.
- Dubrovay Z, Háda V, Béni Z, Szántay C. NMR and mass spectrometric characterization of vinblastine, vincristine and some new related impurities part I. J Pharm Biomed Anal. 2013;84:293–308. https://doi.org/10.1016/j.jpba.2012.08.019.

- 86. Háda V, Dubrovay Z, Lakó-Futó Á, et al. NMR and mass spectrometric characterization of vinblastine, vincristine and some new related impurities—part II. *J Pharm Biomed Anal.* 2013;84:309–322. https://doi.org/10.1016/j.jpba.2012.09.008.
- 87. Kumar A, Patil D, Rajamohanan PR, Ahmad A. Isolation, purification and characterization of vinblastine and vincristine from endophytic fungus fusarium oxysporum isolated from catharanthus roseus. *PLoS One*. 2013;8(9):e71805. https://doi.org/10.1371/journal.pone.0071805.
- Liu M, Mirza A, McAndrew PC, et al. Determination of ligand-binding affinity (Kd) using transverse relaxation rate (R2) in the ligand-observed 1H NMR experiment and applications to fragment-based drug discovery. *J Med Chem.* 2023;66 (15):10617–10627. https://doi.org/10.1021/acs.jmedchem.3c00758.
- 89. Loo TW, Bartlett MC, Clarke DM. Drug binding in human P-glycoprotein causes conformational changes in both nucleotide-binding domains. *J Biol Chem.* 2003;278:1575–1578. https://doi.org/10.1074/jbc.M211307200.
- 90. Kondrashov DA, Van Wynsberghe AW, Bannen RM, Cui Q. Phillips GN. Protein structural variation in computational models and crystallographic data. *Structure*. 2007;15(2):169–177. https://doi.org/10.1016/j.str.2006.12.006.
- Li M, Dang D, Liu L, Xi N, Wang Y. Imaging and force recognition of single molecular behaviors using atomic force microscopy. Sensors. 2017;17(1):200. https://doi.org/10.3390/s17010200.
- 92. Schaefer KG, Roberts AG, King GM. Advantages and potential limitations of applying AFM kymograph analysis to pharmaceutically relevant membrane proteins in lipid bilayers. *Sci Rep.* 2023;13(1):11427. https://doi.org/10.1038/s41598-023-37910-7.
- Lai JI, Tseng YJ, Chen MH, Huang CYF, Chang PMH. Clinical perspective of FDA approved drugs with P-glycoprotein inhibition activities for potential cancer therapeutics. Front Oncol. 2020;10. Accessed April 28, 2023; https://www.frontiersin.org/articles/10.3389/fonc.2020.561936.
- Romsicki Y, Sharom FJ. The membrane lipid environment modulates drug interactions with the P-glycoprotein multidrug transporter. *Biochemistry*. 1999;38:6887–6896.
- 95. Nosol K, Romane K, Irobalieva RN, et al. Cryo-EM structures reveal distinct mechanisms of inhibition of the human multidrug transporter ABCB1. *Proc Nat Acad Sci.* 2020;117(42):26245–26253. https://doi.org/10.1073/pnas.2010264117.
- 96. Pierré A, Pérez V, Léonce S, et al. Relationship between the cellular accumulation and the cytotoxicity of S12363, a new Vinca alkaloid derivative. *Cancer Chemother Pharmacol.* 1992;29(5):367–374. https://doi.org/10.1007/BF00686005.
- 97. Liu Y, Yang X, Gan J, Chen S, Xiao ZX, Cao Y. CB-Dock2: improved protein—ligand blind docking by integrating cavity detection, docking and homologous template fitting. *Nucleic Acids Res.* 2022;50(W1):W159–W164. https://doi.org/10.1093/nar/gkac394.
- Laskowski RA, Swindells MB. LigPlot+: multiple ligand-protein interaction diagrams for drug discovery. Published online 2011.
- Pan L, Aller SG. Allosteric role of substrate occupancy toward the alignment of P-glycoprotein nucleotide binding domains. *Sci Rep.* 2018;8(1):1–14. https://doi.org/10.1038/s41598-018-32815-2.
- Clouser AF, Atkins WM. Long range communication between the drug-binding sites and nucleotide binding domains of the efflux transporter ABCB1. *Biochemistry*. 2022;61(8):730–740. https://doi.org/10.1021/acs.biochem.2c00056.

- Crowley E, O'Mara ML, Reynolds C, et al. Transmembrane helix 12 modulates progression of the ATP catalytic cycle in ABCB1. *Biochemistry*. 2009;48(26):6249–6258. https://doi.org/10.1021/bi900373x.
- 102. Crowley E, O'Mara ML, Kerr ID, Callaghan R. Transmembrane helix 12 plays a pivotal role in coupling energy provision and drug binding in ABCB1. FEBS J. 2010;277(19):3974–3985. https://doi.org/10.1111/j.1742-4658.2010. 07789.x.
- 103. Chai AB, Callaghan R, Gelissen IC. Regulation of P-glycoprotein in the brain. Int J Mol Sci. 2022;23(23):14667. https://doi.org/10.3390/ijms232314667.
- 104. Tran NNB, Bui ATA, Jaramillo-Martinez V, Weber J, Zhang Q. Urbatsch IL. Lipid environment determines the drug-stimulated ATPase activity of P-glycoprotein. Front Mol Biosci. 2023;10.. Accessed April 20, 2023; https://www.frontiersin.org/ articles/10.3389/fmolb.2023.1141081.
- 105. Al-Shawi MK, Polar MK, Omote H, Figler RA. Transition state analysis of the coupling of drug transport to ATP hydrolysis by P-glycoprotein *. *J Biol Chem*. 2003;278(52):52629–52640. https://doi.org/10.1074/jbc.M308175200.
- 106. Sharom FJ. Complex interplay between the P-glycoprotein multidrug efflux pump and the membrane: Its role in modulating protein function. *Front Oncol.* 2014;4 (41):1–19. https://doi.org/10.3389/fonc.2014.00041.
- Thangapandian S, Kapoor K, Tajkhorshid E. Probing cholesterol binding and translocation in P-glycoprotein. *Biochimica et Biophysica Acta (BBA) - Biomembranes*. 2020;1862(1): 183090. https://doi.org/10.1016/j.bbamem.2019.183090.
- Li-Blatter X, Nervi P, Seelig A. Detergents as intrinsic P-glycoprotein substrates and inhibitors. Biochimica et Biophysica Acta (BBA) - Biomembranes. 2009;1788 (10):2335–2344. https://doi.org/10.1016/j.bbamem.2009.07.010.
- 109. Han ES, Zhang JT. Membrane orientation of carboxyl-terminal half P-glycoprotein: Topogenesis of transmembrane segments. Eur J Cell Biol. 1999;78(9):624–631. https://doi.org/10.1016/S0171-9335(99)80047-8.
- Song J, Melera PW. Transmembrane domain (TM) 9 represents a novel site in P-glycoprotein that affects drug resistance and cooperates with TM6 to mediate [1251]lodoarylazidoprazosin Labeling. *Mol Pharmacol*. 2001;60(2):254–261. https://doi.org/10.1124/mol.60.2.254.
- Médioni J, Di Palma M, Guillot A, Spaeth D, Théodore C. Efficacy and safety of Vinflunine for advanced or metastatic urothelial carcinoma in routine practice based on the French multi-centre CURVE study. BMC Cancer. 2016;16:217. https://doi. org/10.1186/s1285-016-2262-9.
- 112. Bachner M, De Santis M. Vinflunine in the treatment of bladder cancer. *Ther Clin Risk Manag.* 2008;4(6):1243–1253.
- P-Glycoprotein Seelig A. One mechanism, many tasks and the consequences for pharmacotherapy of cancers. Front Oncol. 2020;10:1989. https://doi.org/10.3389/ fonc.2020.576559.
- 114. Gherbovet O, Sánchez-Murcia P A, Alvarez MCG, et al. Synthesis and evaluation of hybrid molecules targeting the vinca domain of tubulin. *Org Biomol Chem*. 2015;13(10):3144–3154. https://doi.org/10.1039/C40B02114B.
- Demain AL, Zhang L. Natural products and drug discovery. In: Zhang L. Demain AL, eds. Natural Products. Humana Press; 2005:3–29. https://doi.org/10.1007/978-1-59259-976-9_1.